The Astrophysical Journal, 636:777–797, 2006 January 10


# THE H.E.S.S. SURVEY OF THE INNER GALAXY IN VERY HIGH ENERGY GAMMA RAYS

F. Aharonian,[1,2] A. G. Akhperjanian,[3] A. R. Bazer-Bachi,[4] M. Beilicke,[5] W. Benbow,[2] D. Berge,[2] K. Bernlöhr,[2,6] C. Boisson,[7] O. Bolz,[2] V. Borrel,[4] I. Braun,[2] F. Breitling,[6] A. M. Brown,[8] P. M. Chadwick,[8] L.-M. Chounet,[9] R. Cornils,[5] L. Costamante,[2,10] B. Degrange,[9] H. J. Dickinson,[8] A. Djannati-Ataï,[11] L. O'C. Drury,[12] G. Dubus,[9] D. Emmanoulopoulos,[13] P. Espigat,[11] F. Feinstein,[14] G. Fontaine,[9] Y. Fuchs,[15] S. Funk,[1,2] Y. A. Gallant,[14] B. Giebels,[9] S. Gillessen,[2] J. F. Glicenstein,[16] P. Goret,[16] C. Hadjichristidis,[8] M. Hauser,[13] G. Heinzelmann,[5] G. Henri,[15] G. Hermann,[2] J. A. Hinton,[2] W. Hofmann,[2] M. Holleran,[17] D. Horns,[2] A. Jacholkowska,[14] O. C. de Jager,[17] B. Khélifi,[2] Nu. Komin,[6] A. Konopelko,[2,6] I. J. Latham,[8] R. Le Gallou,[8] A. Lemière,[11] M. Lemoine-Goumard,[9] N. Leroy,[9] T. Lohse,[6] J. M. Martin,[7] O. Martineau-Huynh,[18] A. Marcowith,[4] C. Masterson,[2,10] T. J. L. McComb,[8] M. de Naurois,[18] S. J. Nolan,[8] A. Noutsos,[8] K. J. Orford,[8] J. L. Osborne,[8] M. Ouchrif,[10,18] M. Panter,[2] G. Pelletier,[15] S. Pita,[11] G. Pühlhofer,[2,13] M. Punch,[11] B. C. Raubenheimer,[17] M. Raue,[5] J. Raux,[18] S. M. Rayner,[8] A. Reimer,[19] O. Reimer,[19] J. Ripken,[5] L. Rob,[20] L. Rolland,[18] G. Rowell,[2] V. Sahakian,[3] L. Saugé,[15] S. Schlenker,[6] R. Schlickeiser,[19] C. Schuster,[19] U. Schwanke,[6] M. Siewert,[19] H. Sol,[7] D. Spangler,[8] R. Steenkamp,[21] C. Stegmann,[6] J.-P. Tavernet,[18] R. Terrier,[11] C. G. Théoret,[11] M. Tluczykont,[9,10] G. Vasileiadis,[14] C. Venter,[17] P. Vincent,[18] H. J. Völk,[2] and S. J. Wagner[13]

*Received 2005 June 10; accepted 2005 September 5*

## ABSTRACT

We report on a survey of the inner part of the Galactic plane in very high energy gamma rays with the H.E.S.S. Cerenkov telescope system. The Galactic plane between $\pm 30^\circ$ in longitude and $\pm 3^\circ$ in latitude relative to the Galactic center was observed in 500 pointings for a total of 230 hr, reaching an average flux sensitivity of 2% of the Crab Nebula at energies above 200 GeV. Fourteen previously unknown sources were detected at a significance level greater than 4 $\sigma$ after accounting for all trials involved in the search. Initial results on the eight most significant of these sources were already reported elsewhere (Aharonian and coworkers). Here we present detailed spectral and morphological information for all the new sources, along with a discussion on possible counterparts in other wavelength bands. The distribution in Galactic latitude of the detected sources appears to be consistent with a scale height in the Galactic disk for the parent population smaller than 100 pc, consistent with expectations for supernova remnants and/or pulsar wind nebulae.

*Subject headings:* catalogs — gamma rays: observations — pulsars: general — supernova remnants — supernovae: general — surveys

## 1. INTRODUCTION

Very high energy (VHE, defined here as $E > 10^{11}$ eV) gamma rays provide the most direct view currently available into extreme environments in the local universe. As gamma rays are produced by interactions of relativistic particles, they represent a good probe of nonthermal astrophysical processes. Relativistic electrons can produce gamma rays by nonthermal bremsstrahlung or by inverse Compton scattering on background radiation fields, whereas protons (and atomic nuclei) can generate gamma rays via the decay of neutral pions produced in hadronic interactions with ambient material. VHE gamma radiation is therefore expected from the acceleration sites of particles with energies above 1 TeV ($10^{12}$ eV). In particular, gamma rays can be seen as a probe of sources of nucleonic cosmic rays in our Galaxy and may thus provide part of the solution to the century old puzzle of the origin of this radiation.

[1] Correspondence and request for material should be sent to S. Funk, stefan.funk@mpi-hd.mpg.de.
[2] Max-Planck-Institut für Kernphysik, Saupfercheckweg 1, Postfach 10 39 80, D-69029 Heidelberg, Germany.
[3] Yerevan Physical Institute, Alikhanian Broothers Street, 375036 Yerevan, Armenia.
[4] Centre d'Etude Spatiale des Rayonnements, CNRS/UPS, Toulouse, France.
[5] Universität Hamburg, Institut für Experimentalphysik, Luruper Chaussee 149, D-22761 Hamburg, Germany.
[6] Institut für Physik, Humboldt-Universität zu Berlin, D-10115 Berlin, Germany.
[7] Laboratoire de l'Univers et de ses theories, UMR 8102 du CNRS, Observatoire de Paris, Section de Meudon, France.
[8] University of Durham, Department of Physics, South Road, Durham DH1 3LE, UK.
[9] Laboratoire Leprince-Ringuet, IN2P3/CNRS, Ecole Polytechnique, Palaiseau, France.
[10] European Associated Laboratory for Gamma-Ray Astronomy, jointly supported by CNRS and MPG.
[11] Physique Corpusculaire et Cosmologie, Collège de France, Paris, France.
[12] School of Cosmic Physics, Dublin Institute for Advanced Studies, 5 Merrion Square, Dublin 2, Ireland.
[13] Landessternwarte Heidelberg, Königstuhl, Heidelberg, Germany.
[14] Laboratoire de Physique Théorique et Astroparticules, IN2P3/CNRS, Université Montpellier II, France.
[15] Laboratoire d'Astrophysique de Grenoble, INSU/CNRS, Université Joseph Fourier, France.
[16] DAPNIA/DSM/CEA, CE Saclay, Gif-sur-Yvette, France.
[17] Unit for Space Physics, North-West University, Potchefstroom, South Africa.
[18] Laboratoire de Physique Nucléaire et de Hautes Energies, Universités Paris VI & VII, France.
[19] Institut für Theoretische Physik, Lehrstuhl IV, Ruhr-Universität Bochum, Germany.
[20] Institute of Particle and Nuclear Physics, Charles University, Prague, Czech Republic.
[21] University of Namibia, P.O. Box 86628, Windhoek, Namibia.

Observations of synchrotron emission in the X-ray band provide strong indirect evidence for the existence of $\sim$100 TeV electrons in shell-type supernova remnants (SNRs; see, e.g., Koyama et al. 1995) and in pulsar wind nebulae (PWNs; see, e.g., Weisskopf et al. 2000). At TeV energies, shell-type SNRs and pulsars are established to be sources of VHE gamma rays as shown by highly significant detections of the Crab Nebula by the Whipple collaboration (Weekes et al. 1989) or the detection of the SNR RX J1713.7−3946 by the CANGAROO (Enomoto et al. 2002) and the High Energy Stereoscopic System (H.E.S.S.) collaborations (Aharonian et al. 2004c). However, despite the fact that SNRs are the best candidates for the acceleration of hadronic cosmic rays up to the so-called *knee* in the cosmic-ray particle spectrum at $\sim 10^{15}$ eV, there is as yet no generally accepted evidence for the existence of energetic nuclei (as opposed to electrons) in these objects. SNRs are favored as the site of cosmic-ray acceleration for two principal reasons: (1) a theoretically well-established acceleration mechanism exists in the form of diffusive shock acceleration at SNR shock fronts (for reviews see, e.g., Blandford & Eichler 1987; Malkov & Drury 2001), and (2) the Galactic supernovae and the resulting SNRs are the only known potential sources that can provide the necessary amount of energy (Ginzburg & Syrovatskii 1964).

To explain the observed energy density of cosmic rays, supernova explosions must convert kinetic energy to energy of relativistic particles with a conversion efficiency $\Theta$ of roughly 0.1–0.2. Theoretical expectations for the gamma-ray emission of SNRs arising from hadronic interactions are given by Drury et al. (1994) as

$$F_\gamma(>E) \sim 9 \times 10^{-11} \Theta \left(\frac{E}{1\ \mathrm{TeV}}\right)^{-1.1} S\ \mathrm{cm}^{-2}\ \mathrm{s}^{-1}, \quad (1)$$

with

$$S = \left(\frac{E_{\mathrm{SN}}}{10^{51}\ \mathrm{ergs}}\right)\left(\frac{d}{1\ \mathrm{kpc}}\right)^{-2}\left(\frac{n}{1\ \mathrm{cm}^{-3}}\right), \quad (2)$$

where $d$ denotes the distance to the object, $n$ is the density of the circumstellar medium, assumed to be uniform, and $E_{\mathrm{SN}}$ is the total kinetic energy released by the supernova. This formula assumes a power-law distribution of cosmic-ray energies with a typical differential photon index of 2.1. Calculations of the photon index give a range of values around the index value 2.0 for a uniform circumstellar medium (Berezhko & Völk 1997) and a rather more extended range of photon index values for supernova explosions into the wind bubble of a very massive progenitor star (Berezhko & Völk 2000).

A typical value for the fraction of kinetic energy converted into cosmic rays is $\Theta E_{\mathrm{SN}} = 1.0 \times 10^{50}$ ergs (Malkov & Drury 2001; Völk et al. 2003). For an SNR at a distance of $d = 1$ kpc expanding into an environment with a typical density of the interstellar medium of $n = 1$ hydrogen atom cm$^{-3}$, a VHE gamma-ray flux of 20% of that from the Crab Nebula is expected. The luminosity $L_0$ of such a source is $7.2 \times 10^{33}$ ergs s$^{-1}$ in the energy range between 0.2 and 10 TeV. One would therefore expect that with the sensitivity level of the H.E.S.S. Galactic plane survey (down to $\sim$2% of the Crab flux) SNRs should be detectable out to a distance of 3 kpc (to be compared to 8.5 kpc to the center of the Galaxy). For larger values of $n$, SNRs should be visible within most of the volume of the Galactic disk.

Other potential sources of VHE gamma rays are pulsars and PWNs. Pulsars, rapidly rotating neutron stars left over after a supernova explosion, are highly magnetized and act like unipolar inductors accelerating particles. The pulsar wind interacts with the ambient medium, generating a shock region where particles are accelerated. Such objects may therefore exhibit a pulsed component of radiation, from the immediate vicinity of the pulsar, together with an unpulsed component from the shock region and beyond. The Crab Nebula is the best-studied object of this class of particle accelerators.

Most of these potential Galactic gamma-ray sources such as SNRs and pulsars are associated with the formation of massive stars and therefore cluster along the Galactic plane, especially concentrated in the direction toward the center of our Galaxy. A total of 91 SNRs and 389 pulsars are cataloged within the inner 60° in Galactic longitude and 6° in Galactic latitude (Green 2004; Manchester et al. 2005). Despite the large number of known SNRs and pulsars in our Galaxy, the actual number of detected VHE gamma-ray sources was until now limited to only a handful of objects (for a review see, e.g., Weekes 2000).

Particle acceleration to multi-TeV energies may also be powered by OB stellar associations, via the *superbubble* mechanism (for a summary see Parizot et al. 2004) and also possibly more directly via the stellar winds of member stars and subsequent interaction (see, e.g., Montmerle 1979; Völk & Forman 1982; White 1985; Benaglia et al. 2001). There are presently two TeV sources that may be linked to such OB associations. TeV J2032+4130, discovered by the HEGRA collaboration (Aharonian et al. 2002a), and HESS J1303−631, a recent discovery by H.E.S.S. (Aharonian et al. 2005d), are in the vicinity of the OB associations Cygnus OB2 and Centaurus OB1, respectively. Both TeV sources remain unidentified (UID) in the sense that there are as yet no clear counterparts of similar size and morphology in other wave bands. These sources might represent a new class of objects distributed along the Galactic plane.

At lower energies, observations by the space-based instrument EGRET in the GeV energy range (Hartman et al. 1999) also revealed a population of sources clustering along the Galactic plane. The limited angular resolution of the EGRET instrument renders an identification of these sources in other wave bands very difficult, and most of these objects remain as yet unidentified.

For all these reasons, a survey of the inner part of the Galaxy provides an efficient way to search for gamma-ray emission in order to investigate properties of source classes and search for yet unknown types of Galactic VHE gamma-ray emitters.

At TeV energies the Milagro water Cerenkov detector (Atkins et al. 2004) and the Tibet air-shower array (Amenomori et al. 2002) have been used to perform large-scale surveys. While these instruments have the advantage of a very wide field of view ($\sim$1 sr), the sensitivity obtained by these surveys is rather limited, reaching a flux limit comparable to the flux of the Crab Nebula, $\sim 3 \times 10^{-10}$ cm$^{-2}$ s$^{-1}$ (for $E > 200$ GeV), in 1 yr of observations. Both surveys covered $\sim 2\pi$ sr of the northern sky and revealed no previously unknown significant gamma-ray sources. However, some evidence for gamma-ray emission was found by the Milagro collaboration from a region in the Cygnus constellation and another region close to the Crab Nebula (Smith et al. 2005). Recently the detection of diffuse emission from the Galactic plane with Milagro has been reported (Fleysher et al. 2005).

The HEGRA instrument was the first array of imaging air Cerenkov telescopes to be used to survey a part of the Galactic plane (Aharonian et al. 2002b). The range of Galactic longitudes $-2° < l < 85°$ was observed; due to the location of HEGRA in the Northern Hemisphere and the resulting large zenith angles for observations of the center of the Galactic plane, the sensitivity was reduced for the central part of the Galaxy and the energy

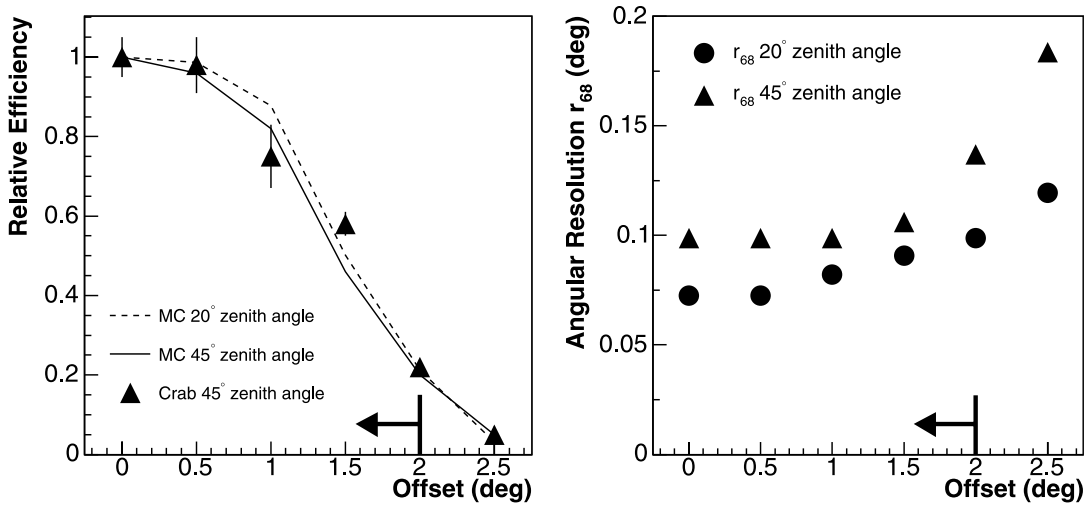


FIG. 1.—Off-axis performance of the H.E.S.S. instrument. *Left*: Gamma-ray efficiency relative to that for an on-axis source for Monte Carlo simulations (*dashed line*: 20° zenith angle; *solid line*: 45° zenith angle) and for H.E.S.S. observations of the Crab Nebula at a mean zenith angle of 47° (*triangles*). The Monte Carlo simulations are generated assuming a Crab-like source spectrum of the form $dN/dE \propto E^{-\Gamma}$ with $\Gamma = 2.5$. *Right*: Simulated angular resolution (68% containment radius) as a function of the offset for observations at zenith angles of 20° (*circles*) and 50° (*triangles*). In each plot the arrow denotes the offset of 2° up to which gamma rays are included in this analysis.

threshold of the observations ranged from 500 GeV to 7 TeV. No sources of VHE gamma rays were found in this survey, and upper limits between 15% of the Crab flux for Galactic longitudes $l > 30°$ and more than 30% of the Crab flux in the inner part of the Milky Way were derived.

Until the completion of H.E.S.S. (Hinton 2004) in early 2004, no VHE gamma-ray survey of comparable sensitivity of the southern sky or of the central region of the Galaxy had been performed. In this paper we describe a survey of this region with H.E.S.S. between 2004 May and July at a flux sensitivity down to 2% of the Crab flux. The initial results from the survey including the description of the discovery of eight new sources have been summarized in Aharonian et al. (2005f). This work presents detailed results on these eight sources. In addition, we report the detection of six additional weaker sources of VHE gamma rays extending to lower flux levels than our previous analysis. Spectral information and a more detailed study on the morphologies for all sources are provided. The paper is structured as follows: After a description of the H.E.S.S. instrument (§ 2) and the Galactic survey data set used in this paper (§ 3), the data analysis technique is presented in § 4. In § 5 we give a detailed description of the individual sources along with possible counterparts in other wave bands, followed by a discussion of the results in § 6 and some conclusions in § 7.

## 2. THE H.E.S.S. INSTRUMENT

H.E.S.S. is a system of four imaging atmospheric Cerenkov telescopes, located in the Khomas Highlands of Namibia at a height of 1800 m above sea level. H.E.S.S. has unprecedented sensitivity in the energy range from 100 GeV to several tens of TeV. The imaging Cerenkov technique exploits the cascade of secondary particles produced in interactions of primary gamma rays with molecules in the Earth's upper atmosphere. These secondary particles emit Cerenkov light, which can be imaged by the Cerenkov telescopes. The energy and direction of the primary gamma rays can be reconstructed based on the intensity and shape of the detected Cerenkov light distribution.

Multiple views of the same particle shower with several telescopes improve background rejection capability and the angular and energy resolution of the instrument, in comparison to a single telescope. Therefore, H.E.S.S. observations are performed in a stereoscopic mode, whereby at least two of the four telescopes must be triggered by a shower for an event to be recorded (Funk et al. 2004). The telescopes each have a mirror area of 107 $m^2$ (Bernlöhr et al. 2003; Cornils et al. 2003). The Cerenkov light is focused onto fast 960 pixel photomultiplier cameras, which record the Cerenkov light images (Vincent et al. 2003). The 5° diameter field of view of the H.E.S.S. cameras is the largest of all imaging Cerenkov detectors and is especially suited for the study of extended sources and the search for unknown sources in surveys. This was part of the original design concept for the H.E.S.S. telescope system (Aharonian et al. 1997b, 1997c).

The H.E.S.S. instrument has an energy threshold of ~100 GeV at zenith before selection cuts, an angular resolution of ~0°.1 for individual gamma rays, and a point source sensitivity of $<2.0 \times 10^{-13}$ cm$^{-2}$ s$^{-1}$ above 1 TeV (1% of the flux from the Crab Nebula) for a 5 $\sigma$ detection in a 25 hr observation. The sensitivity of H.E.S.S. and the capability to map large extended sources have been demonstrated by the resolved images of the SNRs RX J1713.7−3946 (Aharonian et al. 2004c) and RX J0852.0−4622 (Aharonian et al. 2005c). The serendipitous detections of the unidentified source HESS J1303−631 in the field of view of the binary pulsar PSR B1259−63 and of the composite SNR G0.9+0.1 (Aharonian et al. 2005b) in the field of view of the Galactic center source HESS J1745−290 (Aharonian et al. 2004a) demonstrate the advantage of a large field of view. This large field of view implies that some sources are observed up to 2° off the optical axis of the telescope system.

To illustrate the off-axis performance within the field of view of H.E.S.S., Figure 1 summarizes some basic parameters as a function of the offset. The left panel shows the gamma-ray efficiency relative to on-axis pointing, derived from Monte Carlo simulations for two different zenith angles along with measurements of the Crab Nebula. The plot shows a weak dependence of the gamma-ray efficiency on zenith angle and reasonable agreement between Monte Carlo simulations and data. The right panel of Figure 1 shows the angular resolution of H.E.S.S. (specified by the 68% containment radius of the point-spread function [PSF]) versus offset in the camera for observations at two different zenith angles. It is

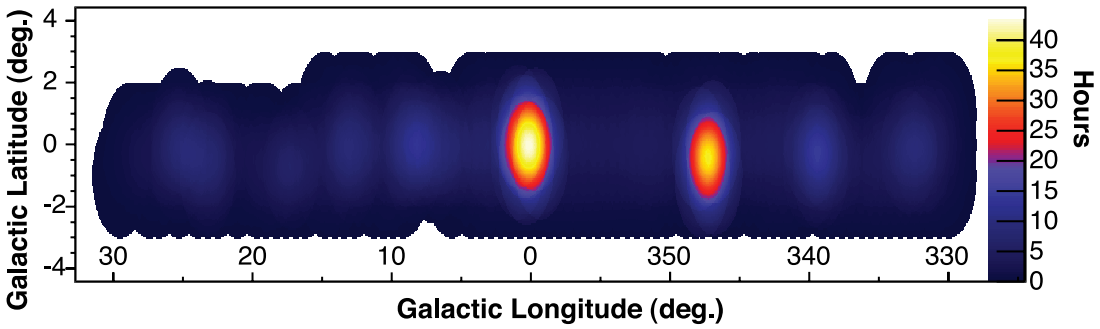


FIG. 2.—Effective exposure of the H.E.S.S. Galactic plane survey, expressed as equivalent number of hours spent observing a source at the center of the field of view. The deeper observations of RX J1713.7−3946 and the Galactic center are apparent.

evident that the angular resolution is better than 0.°1 and is reasonably constant in the inner 1.°5 of the field of view.

## 3. THE H.E.S.S. GALACTIC PLANE SURVEY

The survey was conducted in the Galactic longitude band $\pm 30^\circ$ around $l = 0^\circ$. Runs of 28 minute duration were taken at pointing positions with a spacing of 0.°7 in longitude in three strips in Galactic latitude: $b = -1^\circ, 0^\circ$, and $+1^\circ$. For the data analysis runs were selected based on weather and hardware conditions. A total of 95 hr of quality-selected data were taken in the scan mode between 2004 May and July. The observation schedule was optimized so that individual pointings were conducted near culmination, resulting in the smallest zenith angles accessible. Promising source candidates were reobserved between 2004 July and October, yielding a further 30 good-quality hours of data. For the analysis described in the following, additional pointed observations of SNR RX J1713.7−3946 and of the Galactic center region are included. The total data set presented here amounts to 230 hr after quality selection, and the mean zenith angle of all observations is 26°. Figure 2 shows a map of exposure for this data set, expressed in terms of an equivalent number of hours observing a source at the center of the field of view.

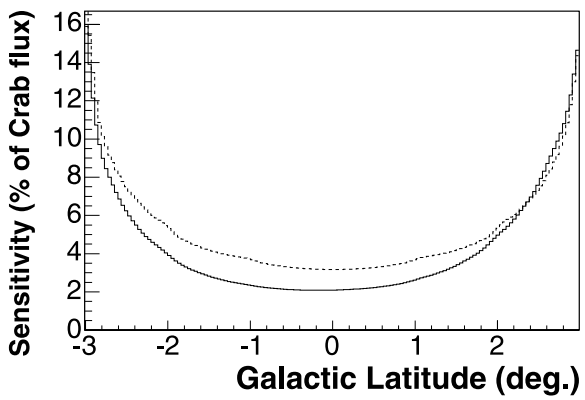


FIG. 3.—Sensitivity in Galactic latitude of the H.E.S.S. Galactic plane scan in units of the flux from the Crab Nebula ($\sim 3 \times 10^{-10}$ cm$^{-2}$ s$^{-1}$, $E > 200$ GeV) and assuming a power-law spectrum with photon index $\Gamma = 2.5$. The sensitivity used here is defined as the minimum flux of a point source that would be detectable in this survey by H.E.S.S. at the 6.3 $\sigma$ level (corresponding to 4 $\sigma$ after accounting for all trials), given the cuts used to detect slightly extended sources (in particular a $\theta^2 = 0.05$ deg$^2$ cut). The solid line shows the sensitivity averaged over the whole longitude range of the survey, including runs on the Galactic center region and on the SNR RX J1713.7−3946. The dashed line shows the sensitivity in the range of longitude $350^\circ < l < 357^\circ$, a region where no reobservations were conducted.

As can be seen from Figure 2, the exposure is not uniform with peak exposures in the regions around RX J1713.7−3946 and the Galactic center. This irregular exposure results in an uneven sensitivity for the detection of new sources. The sensitivity of the survey in Galactic latitude (averaged over the whole longitude range) is shown in Figure 3. For $-1.^\circ5 < b < 1.^\circ5$ the sensitivity is rather flat at a level of 2% of the flux from the Crab Nebula and deteriorates rapidly at $>2^\circ$ from the Galactic plane. The flux sensitivity above 200 GeV is ~50% worse for a source with photon index $\Gamma = 3.0$ compared to one with $\Gamma = 2.0$.

## 4. DATA ANALYSIS

Following calibration of the data (Aharonian et al. 2004b), the standard H.E.S.S. event reconstruction scheme was applied to the data set. After tail-cut image cleaning and a Hillas parameterization algorithm, the direction of the shower axis was reconstructed by intersection of the major axes of the Hillas ellipses. H.E.S.S. standard cuts (Aharonian et al. 2005a) on the width and length of these ellipses (scaled to the width and length expected from Monte Carlo simulations) were used to suppress the hadronic background. An additional cut on the image size >200 photoelectrons (p.e.) yields optimum sensitivity for weak sources provided that source spectra are not significantly steeper than that of the Crab Nebula. They result in an angular resolution of 0.°08 (68% containment radius) and an energy threshold of 250 GeV. To reduce systematic effects that affect images close to the edge of the camera, only events reconstructed within a maximum distance of 2° from the pointing direction of the system were used for this analysis. The survey region was divided (a priori) into a grid of trial source positions with grid points spaced by 0.°04, a value well below the angular resolution of the instrument. For each grid point in the scan region, the on-source signal was calculated by summing up all events within a circle of radius $\theta = 0.^\circ22$ (or $\theta^2 = 0.05$ deg$^2$), where $\theta$ denotes the angular distance between the reconstructed event direction and the grid point. This cut is appropriate for slightly extended sources with respect to the angular resolution of the instrument and was chosen a priori, since it is optimal for the detection of gamma-ray sources with the average observed size of Galactic SNRs (Green 2004). A search for very extended sources (relative to the angular resolution) using a larger $\theta^2$ cut yields similar results. A similar search for pointlike sources with a $\theta^2 = 0.01$ deg$^2$ cut revealed a subset of the sources presented here and, additionally, the pointlike source HESS J1826−148, which is associated with the microquasar LS 5039. The discovery of this source is reported elsewhere (Aharonian et al. 2005g).

The background for each grid point was estimated using two different techniques. The standard H.E.S.S. background estimation method counts background events in a ring around each grid point

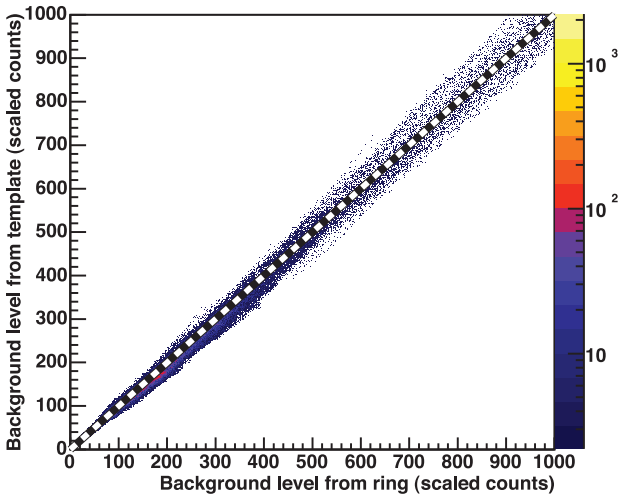


FIG. 4.—Background level estimated for each grid point, calculated using a ring background technique, plotted against the background level estimated from a template method (Rowell 2003). The black dashed line shows the expected one-to-one correlation.

with a mean radius of 0.°5 and an area 7 times that of the on-region to estimate the background level. The standard ring radius of 0.°5 was increased to 0.°6 (again a priori) to improve sensitivity to extended sources. Using appropriate weight factors, this background determination takes into account the difference in system acceptance and exposure for the on- and the off-regions (Aharonian et al. 2005a). An alternative technique uses the *template* approach, where the background level is estimated using events that are normally rejected by the cosmic-ray background rejection criterion based on the scaled image width and length, but with reconstructed directions falling within the on-source region (Rowell 2003). The normalization in this case is determined by the overall ratio of events in both cut regimes, taking into account the ratio of relative acceptances in the two regimes. Figure 4 shows the correlation of the background level estimated for each grid point from the ring background and from the template background method. The slope of the major axis of the distribution is 1.007. This shows that the background estimates are consistent within 1%. The template background seems to slightly underestimate the background in comparison to the ring background. The ring background technique should therefore give a more conservative estimation of the significances of the new sources. In the following the ring background estimation method will be used as the standard method, since it is a robust method in which linear gradients in the system acceptance cancel out.

From the on-counts, the background level, and the relative background acceptance in the system, a statistical significance can be determined for each grid point in the map, testing the existence of a gamma-ray source at the position of that grid point (using the approach of Li & Ma 1983). A number of significant sources are detected, and Table 1 gives the on-counts, the background level as derived from the ring background determination method (after accounting for the difference in acceptance and in the area between the on-source and off-source regions), and the resulting number of gamma-ray excess events. Since the map contains a large number of test positions, this significance has to be corrected according to a "trial factor." This trial factor accounts for the increased probability of finding a fake signal with an increased number of test positions for which a significance is calculated. Using a Monte Carlo simulation of the technique applied to the survey data (including a realistic exposure map and randomly

TABLE 1

ON-SOURCE COUNTS, SCALED BACKGROUND LEVEL ($\alpha N_{\rm off}$ ACCORDING TO THE NOTATION OF LI & MA 1983), AND GAMMA-RAY EXCESS EVENTS FOR THE NEW SOURCES OF VHE GAMMA RAYS DETECTED IN THE SURVEY OF THE GALACTIC PLANE

| Name | On-Counts | Scaled Background | Excess |
|---|---|---|---|
| HESS J1614−518..... | 517 | 283 | 234 |
| HESS J1616−508..... | 766 | 356 | 410 |
| HESS J1632−478..... | 232 | 139 | 93 |
| HESS J1634−472..... | 275 | 175 | 100 |
| HESS J1640−465..... | 611 | 298 | 313 |
| HESS J1702−420..... | 311 | 210 | 101 |
| HESS J1708−410..... | 955 | 728 | 227 |
| HESS J1713−381..... | 917 | 728 | 189 |
| HESS J1745−303..... | 1138 | 927 | 211 |
| HESS J1804−216..... | 887 | 508 | 379 |
| HESS J1813−178..... | 717 | 374 | 343 |
| HESS J1825−137..... | 406 | 232 | 174 |
| HESS J1834−087..... | 478 | 287 | 191 |
| HESS J1837−069..... | 622 | 328 | 294 |

NOTES.—The on-counts are calculated by counting events within a circle of radius $\theta = 0.^\circ22$ centered on the position of the source. The background counts are derived by counting events in a ring around the source position with average radius 0.°6 multiplied with the normalization factor $\alpha \sim \frac{1}{7}$ that takes into account the difference in the acceptance and the area between the on-source and the background region.

generating the events for each run from the acceptance function of that run), it has been found that this trial factor is somewhat lower than the number of points for which a significance is calculated, i.e., the number of grid points in the map ($n = 220{,}000$), since the excess counts for adjacent grid points are correlated, given that the integration radius is larger than the grid spacing. For uncorrelated grid points one would have exactly the factor $n$. For the calculation of post-trial significances we conservatively assume that the number of trials is equal to the number of bins $n$. Figure 5 shows the distribution of significances for all grid points in the map (*solid black line*). The large positive tail to the

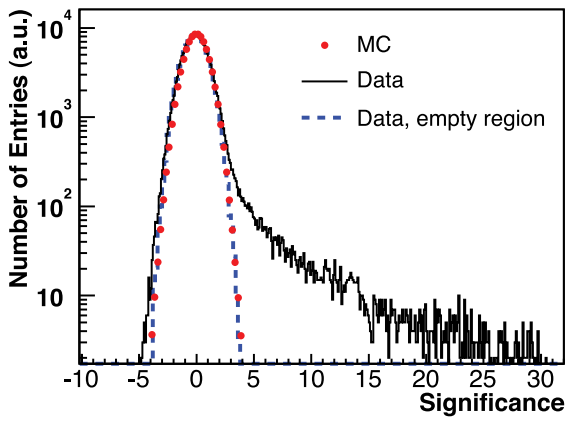


FIG. 5.—Distribution of significances in the survey region (*solid black line*). For comparison, the distribution of significances in a region without gamma-ray sources is shown as a dashed blue line. The distribution of significances for a Monte Carlo simulation of the survey without gamma-ray sources is shown as red filled circles and follows a Gaussian distribution with zero mean and unit width. A Gaussian fit to the dashed blue distribution yields a mean of $-0.050 \pm 0.003$ with an rms of $1.027 \pm 0.001$, indicating a small systematic error in the determination of the significances at the level of a few percent. The dashed blue line and the red data points have been scaled to the peak height of the black distribution.

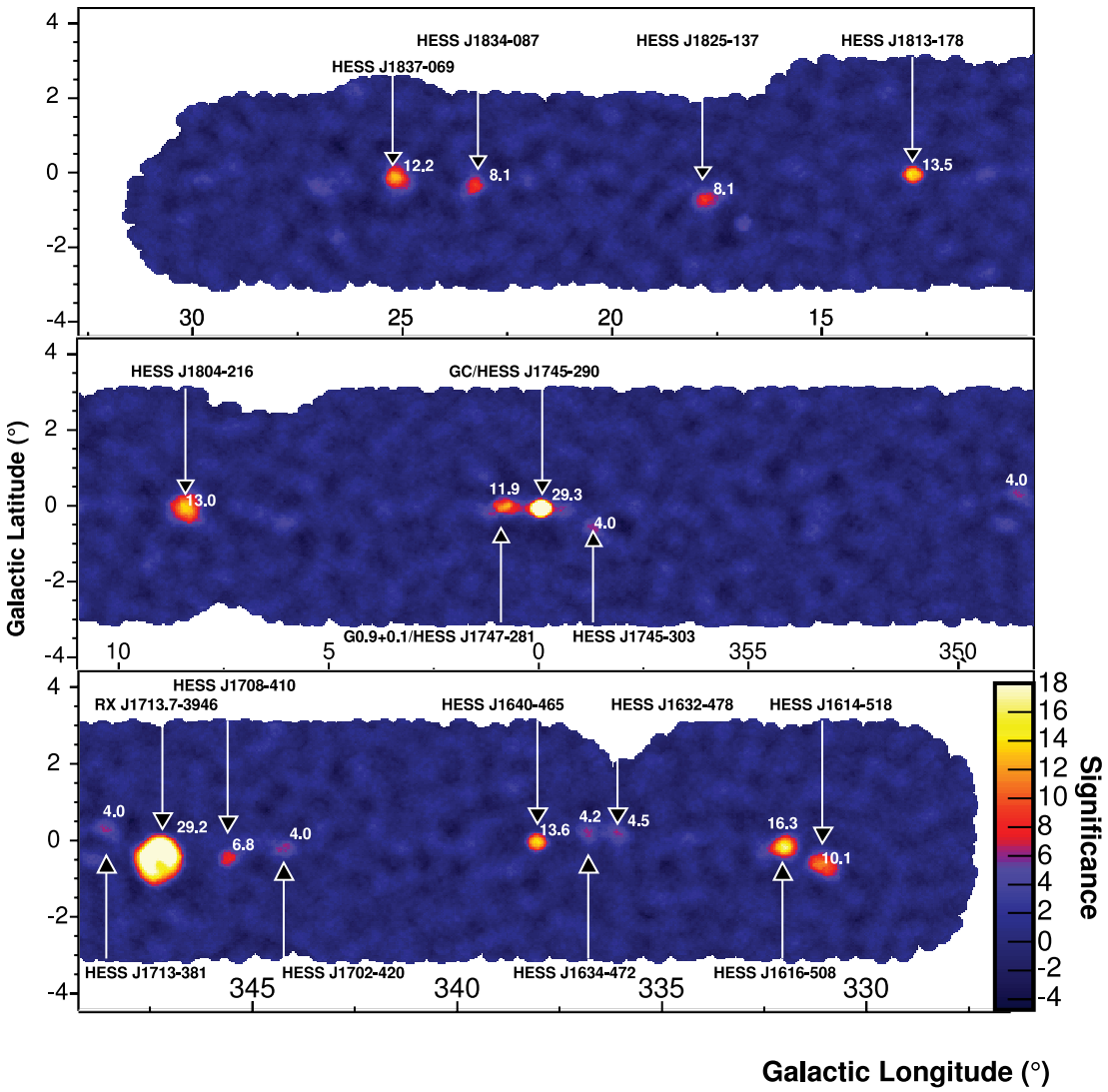


FIG. 6.—Significance map of the H.E.S.S. Galactic plane survey in 2004, including data from reobservations of source candidates detected in the original scan and observations of the known gamma-ray emitter RX J1713.7−3946 and the Galactic center region. The typical energy threshold for this map is 250 GeV. The on-source counts for each grid point are integrated in a circle of radius $\theta = 0.^{\circ}22$. The background for each grid point has been derived using a ring of mean radius $0.^{\circ}6$ and an area 7 times that of the on-source circle. The labels indicate the gamma-ray sources described in this work, along with the known gamma-ray sources RX J1713.7−3946 (HESS J1713−397), G0.9+0.1 (HESS J1747−281), and the Galactic center (HESS J1745−290). The numbers in the map give the post-trial significances of the gamma-ray sources. The significance scale is truncated at 18 $\sigma$; the signals from the Galactic center and RX J1713.7−3946 exceed this level.

distribution can be attributed to the existence of gamma-ray sources. The much smaller tail of negative significances is due to the existence of gamma-ray sources in the regions used for background estimation. This effect has been minimized in a second iteration in which regions of significant gamma-ray excess are excluded as background regions. Also shown in dashed blue is the distribution of significances for a region in the map without significant sources ($l = 0^{\circ} \pm 20^{\circ}$, $0.^{\circ}5 < b < 1.^{\circ}5$). This distribution has been scaled to have the same peak height as the distribution of significances for all grid points (*black*). A Gaussian fit to this distribution yields a mean of $-0.050 \pm 0.003$ with an rms of $1.027 \pm 0.003$, in tolerable agreement with the expected normal Gaussian distribution given the possibility of undetected gamma-ray emission in the on-source or off-source regions. The distribution of significances for a Monte Carlo simulation of the survey without gamma-ray sources, using the same analysis procedure as for data, is shown with red filled circles. This distribution has also been scaled to have the same peak height as the distribution of significances for all grid points (*black*) and is consistent with a normal Gaussian, demonstrating that the analysis technique behaves as expected.

A post-trial significance $S_2$ (the effective *detection significance*) was calculated from the pre-trial significance $S_1$ by converting $S_1$ into a probability, recalculating the probability of the occurrence of one or more such events given the number of trials, and converting this probability back into a significance. Grid points for which the post-trial significance is above 4.0 $\sigma$ (corresponding to 6.3 $\sigma$ before trials) are considered as likely sources of VHE gamma rays and are included in the following discussion. The probability of a single fake signal at this level is $3 \times 10^{-5}$ in the whole survey. Figure 6 shows the map of significances before accounting for the trial factor with the background estimated from the ring technique. The strong gamma-ray sources RX J1713.7−3946 and HESS J1745−290 clearly stand out, partly because of the high exposure in these regions. Also visible at a much fainter level is the recently published new gamma-ray source G0.9+0.1

TABLE 2
SIGNIFICANCES FOR THE NEW SOURCES OF VHE GAMMA RAYS DETECTED IN THE SURVEY OF THE GALACTIC PLANE

| | BEST-FIT POSITION | | | | SIGNIFICANCE | | | |
|---|---|---|---|---|---|---|---|---|
| NAME[a] | $l$ (deg) | $b$ (deg) | R.A. (deg) | Decl. (deg) | $S_1$ | $S_2$ | $S_3$ | LIVE TIME (hr) |
| HESS J1614−518† | 331.52 | −0.58 | 243.58 | −51.82 | 11.2 | 10.1 | 7.5 | 9.8 |
| HESS J1616−508† | 332.39 | −0.14 | 244.10 | −50.90 | 17.1 | 16.3 | 9.7 | 10.2 |
| HESS J1632−478 | 336.38 | 0.19 | 248.04 | −47.82 | 6.6 | 4.5 | ... | 4.5 |
| HESS J1634−472 | 337.11 | 0.22 | 248.74 | −47.27 | 6.4 | 4.2 | 1.8 | 6.6 |
| HESS J1640−465† | 338.32 | −0.02 | 250.18 | −46.53 | 14.5 | 13.6 | 14.5 | 14.3 |
| HESS J1702−420 | 344.26 | −0.22 | 255.69 | −42.07 | 6.3 | 4.0 | 4.1 | 5.7 |
| HESS J1708−410 | 345.67 | −0.44 | 257.06 | −41.08 | 8.4 | 6.8 | 6.9 | 37.4 |
| HESS J1713−381 | 348.65 | 0.38 | 258.49 | −38.20 | 6.3 | 4.0 | 1.4 | 37.3 |
| HESS J1745−303 | 358.71 | −0.64 | 266.26 | −30.37 | 6.3 | 4.0 | 1.8 | 35.3 |
| HESS J1804−216† | 8.40 | −0.03 | 271.13 | −21.70 | 13.9 | 13.0 | 7.7 | 15.7 |
| HESS J1813−178† | 12.81 | −0.03 | 273.40 | −17.84 | 14.4 | 13.5 | 15.3 | 9.7 |
| HESS J1825−137† | 17.82 | −0.74 | 276.51 | −13.76 | 9.5 | 8.1 | 3.7 | 8.4 |
| HESS J1834−087† | 23.24 | −0.32 | 278.69 | −8.76 | 9.5 | 8.1 | 5.7 | 7.3 |
| HESS J1837−069† | 25.18 | −0.11 | 279.41 | −6.95 | 13.2 | 12.2 | 9.9 | 7.6 |

NOTES.—Source positions are derived from a fit to the gamma-ray counts in fine angular bins and do not rely on the coarser spaced search grid. $S_1$ stands for the pre-trial significance (using a $\theta^2$ cut of 0.05 deg$^2$) for the peak positions in the map. $S_2$ shows the post-trial significance for this position. $S_3$ shows the post-trial significance for this position for a point-source cut ($\theta_{\rm point} = 0.^\circ1$).

[a] The sources that are marked with a dagger have been previously reported in Aharonian et al. (2005f).

(Aharonian et al. 2005b), which was serendipitously detected in the H.E.S.S. observations of the Galactic center region. In addition to these three known objects, 14 new sources of VHE gamma rays are detected at a significance level above 4 $\sigma$ (post-trials), the 8 most significant of which have been discussed in a previous publication (Aharonian et al. 2005f ). Table 2 shows the pre-trial significance for the peak positions in the map for the new sources in the sixth column ($S_1$) and the significance after accounting for the number of trials in the seventh column ($S_2$). The eighth column ($S_3$) shows the post-trial significance applying a cut appropriate for point sources ($\theta_{\rm point} = 0.^\circ1$) instead of the extended source cut $\theta = 0.^\circ22$. Only two of the new sources (HESS J1640−465 and HESS J1813−178) show a nonmarginal increase in significance using the point-source cut. The extension of the new sources is discussed in the next section. It should be noted that the five sources with detection significances $S_2$ below 5 $\sigma$ should be considered as source candidates, rather than firmly established sources. Reobservation of these sources will be necessary to confirm these marginal detections.

## 5. CHARACTERISTICS OF THE NEW SOURCES

This section describes the main results and the analysis techniques that were applied to provide information about position, extension, and spectra of the new VHE gamma-ray sources.

### 5.1. *Position and Morphology*

A detailed spectral and positional analysis has been performed on the 14 sources listed in Table 2. For this purpose, the distribution of gamma-ray candidates was determined for fine angular bins of width $0.^\circ005$, to allow for a more accurate determination of the source position. For the position and approximate size determination of each source, the spatial distribution of events in the (uncorrelated) bins was fitted to a model of a two-dimensional Gaussian gamma-ray brightness profile of the form $\rho \propto \exp(-\theta^2/2\sigma^2_{\rm source})$, convolved with the PSF of the instrument, and an added background parameterization. To properly handle the small number of events in the bins, a likelihood fit appropriate for Poisson statistics was applied in this procedure. To test for possible elongation of each emission region, an elongated Gaussian with independent $\sigma_{\rm source}$ and $\sigma'_{\rm source}$ in each dimension and a free orientation angle $\omega$ (measured counterclockwise from the positive Galactic latitude axis) was also fitted. The source is flagged as elongated if the error range in best-fit minor-axis $\sigma'_{\rm source}$ is outside that of the best-fit major-axis $\sigma_{\rm source}$. This fitting procedure has been tested using Monte Carlo simulations under realistic conditions. The reanalysis of the source positions presented here in comparison to Aharonian et al. (2005f ) yields a maximum shift of $2'$–$3'$ for the most extended of these sources, reflecting the more detailed study presented here. The new positions are consistent within errors with the previously published positions. Also the previously reported extensions are confirmed by the more detailed analysis presented here, with the exception of HESS J1834−087, where the extension was overestimated due to the non-Gaussian shape of the source and is now determined to be $0.^\circ09$ rather than $0.^\circ20$.

The system PSF (see Fig. 1) has been derived from Monte Carlo simulations as a function of the zenith angle of observations and of the offset of a source in the field of view. This model PSF is consistent with the excesses observed for the pointlike Crab Nebula and the active galaxy PKS 2155−304 (Aharonian et al. 2005a). Table 3 shows the best-fit position, the best-fit Gaussian equivalent sizes $\sigma_{\rm source}$ and $\sigma'_{\rm source}$, and the orientation $\omega$ (in case of elongation) of the 14 sources. To quantify the quality of the fit, the last column of Table 3 shows the normalized $\chi^2$ between the model source shape and the measured radial profile for each source.

Figure 7 shows the distribution of sizes for the new sources. For the elongated sources, the arithmetic mean of $\sigma_{\rm source}$ and $\sigma'_{\rm source}$ has been filled into the histogram. All but two of the sources appear significantly extended above a level of three standard deviations. Four out of 14 appear significantly elongated, whereas the remaining 10 new sources are compatible with a radially symmetric shape. The radial excess distributions of all sources are given individually in § 5.3.

### 5.2. *Spectra*

Using the best-fit position, a spectral analysis was performed, again assuming a Gaussian emission region and using a cut of

TABLE 3
Position and Sizes of the New Sources of VHE Gamma Rays Detected in the Survey of the Galactic Plane

| Name | Best-Fit Position $l$ (deg) | Best-Fit Position $b$ (deg) | $\sigma_{source}$ (deg) | $\sigma'_{source}$ (deg) | $\omega$ (deg) | $\chi^2_{norm}$ |
|---|---|---|---|---|---|---|
| J1614−518..... | 331.52 ± 0.03 | −0.58 ± 0.02 | 0.23 ± 0.02 | 0.15 ± 0.02 | 49 ± 10 | 1.44 |
| J1616−508..... | 332.391 ± 0.014 | −0.138 ± 0.013 | 0.136 ± 0.008 | ... | ... | 0.82 |
| J1632−478..... | 336.38 ± 0.04 | 0.19 ± 0.03 | 0.21 ± 0.05 | 0.06 ± 0.04 | 21 ± 13 | 1.05 |
| J1634−472..... | 337.11 ± 0.05 | 0.22 ± 0.04 | 0.11 ± 0.03 | ... | ... | 0.72 |
| J1640−465..... | 338.316 ± 0.007 | −0.021 ± 0.007 | 0.045 ± 0.009 | ... | ... | 0.91 |
| J1702−420..... | 344.26 ± 0.04 | −0.22 ± 0.03 | 0.08 ± 0.04 | ... | ... | 1.38 |
| J1708−410..... | 345.672 ± 0.013 | −0.438 ± 0.010 | 0.054 ± 0.012 | ... | ... | 0.86 |
| J1713−381..... | 348.65 ± 0.03 | 0.38 ± 0.03 | 0.06 ± 0.04 | ... | ... | 1.04 |
| J1745−303..... | 358.71 ± 0.04 | −0.64 ± 0.05 | 0.21 ± 0.06 | 0.09 ± 0.04 | 54 ± 7 | 1.17 |
| J1804−216..... | 8.401 ± 0.016 | −0.033 ± 0.018 | 0.200 ± 0.010 | ... | ... | 1.34 |
| J1813−178..... | 12.813 ± 0.005 | −0.0342 ± 0.005 | 0.036 ± 0.006 | ... | ... | 0.94 |
| J1825−137..... | 17.82 ± 0.03 | −0.74 ± 0.03 | 0.16 ± 0.02 | ... | ... | 1.03 |
| J1834−087..... | 23.24 ± 0.02 | −0.32 ± 0.02 | 0.09 ± 0.02 | ... | ... | 1.16 |
| J1837−069..... | 25.185 ± 0.012 | −0.106 ± 0.016 | 0.12 ± 0.02 | 0.05 ± 0.02 | 149 ± 10 | 1.52 |

Notes.—Galactic longitude $l$ and latitude $b$, the rms source size $\sigma_{source}$ and $\sigma'_{source}$, and the orientation angle $\omega$ counterclockwise with respect to the positive Galactic latitude axis are given in degrees. Parameter $\chi^2_{norm}$ denotes the normalized $\chi^2$, with 49 degrees of freedom.

$\theta^2 < \theta^2_{point}(\sigma^2_{source}+\sigma^2_{PSF})/\sigma^2_{PSF}$, approximating the H.E.S.S. PSF as a two-dimensional Gaussian with $\sigma_{PSF} = 0.^\circ08$ and $\theta_{point} = 0.^\circ1$ being the optimal cut for point sources. Such a cut provides optimum significance for a weak Gaussian-shaped source on a uniform background and hence the best possible spectral determination. For the elongated sources, the larger of the two values $\sigma_{source}$ and $\sigma'_{source}$ was used. The energy-dependent efficiency of this $\theta$ cut is estimated by convolving the H.E.S.S. PSF with a Gaussian of size $\sigma_{source}$. This introduces an additional systematic error in the absolute flux determination since it implicitly assumes that the emission region of the source follows a Gaussian distribution and that the morphology of the source does not show any energy dependency. The typical overall systematic error in the determination of the integral flux level is estimated to be ∼30%. The standard H.E.S.S. spectral analysis technique is described in Aharonian et al. (2005a). To avoid systematic errors in the spectral determination arising from different camera acceptances across the H.E.S.S. field of view, the spectral background determination employs regions of the same size and shape as the on-region, but displaced on a ring in the field of view around the camera center. The ring was chosen such that the off-regions have the same angular distance to the center as the on-region. This approach ensures that background events are taken at the same zenith and offset angles.

To keep as many low-energy gamma rays as possible, a looser size cut of 80 photoelectrons is used in the spectral analysis. This cut allows us to reach a lower energy threshold (150 GeV) at the expense of reduced sensitivity for hard-spectrum sources and a 30% poorer angular resolution. Flux points below a significance level of 2 standard deviations were discarded in the spectral analysis, and the binning was doubled at high energies for weak sources. Table 4 lists the resulting photon index Γ and flux above 200 GeV for a power-law fit $dN/dE = F_0E^{-\Gamma}$. The typical systematic error on these photon indices is estimated to be ∼0.2. It should be noted that the fluxes reported here are in general different

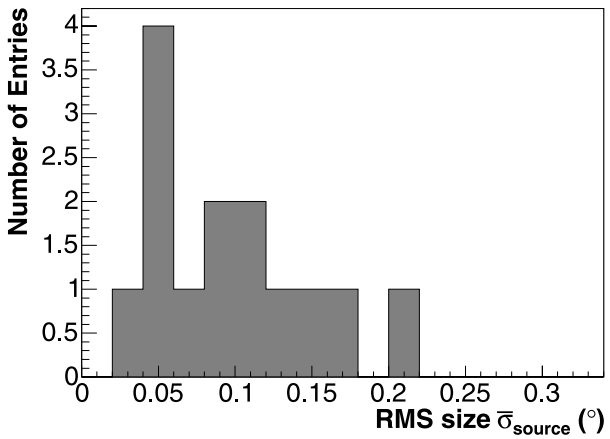


Fig. 7.—Distribution of the rms angular size $\sigma_{source}$ of the 14 VHE gamma-ray sources. For the elongated sources, the arithmetic mean of $\sigma_{source}$ and $\sigma'_{source}$ is used. The mean of this distribution is $0.^\circ1$ with an rms of $0.^\circ05$.

TABLE 4
Results of a Power-Law Fit $dN/dE = F_0E^{-\Gamma}$ for the 14 Sources of VHE Gamma Rays

| Name | Γ | Flux > 200 GeV ($10^{-12}$ cm$^{-2}$ s$^{-1}$) | $\theta$ Cut (deg) | $\chi^2$/dof |
|---|---|---|---|---|
| HESS J1614−518..... | 2.46 ± 0.20 | 57.8 ± 7.7 | 0.40 | 0.6/3 |
| HESS J1616−508..... | 2.35 ± 0.06 | 43.3 ± 2.0 | 0.26 | 5.5/5 |
| HESS J1632−478..... | 2.12 ± 0.20 | 28.7 ± 5.3 | 0.36 | 7.9/2 |
| HESS J1634−472..... | 2.38 ± 0.27 | 13.4 ± 2.6 | 0.23 | 5.8/5 |
| HESS J1640−465..... | 2.42 ± 0.15 | 20.9 ± 2.2 | 0.16 | 3.7/4 |
| HESS J1702−420..... | 2.31 ± 0.15 | 15.9 ± 1.8 | 0.20 | 7.8/6 |
| HESS J1708−410..... | 2.34 ± 0.11 | 8.8 ± 0.7 | 0.17 | 6.3/3 |
| HESS J1713−381..... | 2.27 ± 0.48 | 4.2 ± 1.5 | 0.17 | 1.8/2 |
| HESS J1745−303..... | 1.82 ± 0.29 | 11.2 ± 4.0 | 0.36 | 4.4/3 |
| HESS J1804−216..... | 2.72 ± 0.06 | 53.2 ± 2.0 | 0.36 | 6.9/11 |
| HESS J1813−178..... | 2.09 ± 0.08 | 14.2 ± 1.1 | 0.15 | 5.5/11 |
| HESS J1825−137..... | 2.46 ± 0.08 | 39.4 ± 2.2 | 0.30 | 6.2/8 |
| HESS J1834−087..... | 2.45 ± 0.16 | 18.7 ± 2.0 | 0.20 | 3.5/4 |
| HESS J1837−069..... | 2.27 ± 0.06 | 30.4 ± 1.6 | 0.23 | 12.6/10 |

Notes.—The $\theta$ cut used for the spectral analysis is given in degrees. The errors given on the photon index and flux are statistical only. The typical systematic errors are ∼0.2 in the photon index and ∼30% in the absolute flux. To derive a combined error on the photon index, the systematic and statistical errors should be added in quadrature.

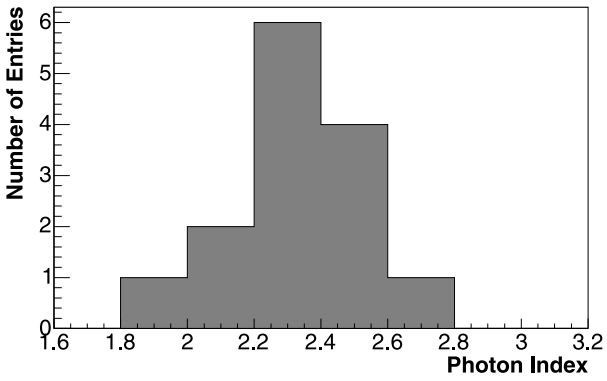


FIG. 8.—Distributions of the photon index of the new sources. The mean photon index is 2.32 with an rms of 0.2.

from the fluxes reported in Aharonian et al. (2005f) (especially for the larger sources) since in the present work the flux is determined from a larger region, adapted to encompass a larger fraction of the emission region, whereas in Aharonian et al. (2005f), a fixed small $\theta^2 = 0.02$ deg$^2$ cut was used for all sources.

Figure 8 shows the distribution of photon indices for the 14 new sources. The distribution exhibits a mean of 2.32, marginally consistent with predictions by models of shock wave acceleration in SNRs (see, e.g., Berezhko & Völk 1997, 2000) and as expected for the source spectrum of Galactic cosmic rays (see, e.g., Jones et al. 2001). The distribution has an rms of 0.2, comparable with the statistical errors on the measurements.

### 5.3. *Individual Gamma-Ray Sources*

This section describes the 14 VHE gamma-ray sources detected in the Galactic plane survey individually along with a brief description of possible counterparts at other wavelengths. Excess maps are shown that have been smoothed with a two-dimensional Gaussian to reduce the effect of statistical fluctuations. The resulting count map is in units of integrated excess counts within the smoothing radius. The rms radius of the Gaussian used for the smoothing is adapted for each source according to the available photon statistics. This radius is given in the figure captions and is shown as a dotted black line in the inset in the lower right part of each excess map along with the PSF of the instrument, smoothed in the same way as the excess map. Note that the maps have different scales; therefore, the white line in the upper right corner indicates a $0.^{\circ}2$ scale. Further, it should be noted that the color scale covers different intervals for different maps.

Also shown are possible counterparts to the VHE gamma-ray emission: SNR from Green (2004) (with white circles illustrating their nominal radii), pulsars from the ATNF pulsar catalog (Manchester et al. 2005; *white triangles*), hard X-ray sources detected by the *International Gamma-Ray Astrophysics Laboratory* (*INTEGRAL*) satellite (*white stars*), and unidentified EGRET sources from the third EGRET catalog (Hartman et al. 1999) (showing the 95% error contour for the position of the source in dashed white). In some maps contours of radio and/or X-ray emission are also shown and discussed individually. The 20 cm Very Large Array (VLA) radio contours are taken from White et al. (2005). The X-ray *ASCA* data show smoothed count maps obtained with the GIS instrument in the 0.7–10 keV band. The best-fit source position of the H.E.S.S. source is shown with error bars in black, and the best-fit (Gaussian) source size is shown as a black dashed circle or ellipse. The radial distribution of gamma-ray excess with respect to the best-fit source position is shown for each source binned appropriately for the available photon statistics; in each plot the number of reconstructed events in bins of the squared angular distance ($\theta^2$) is shown along with the best-fit radially symmetric model (*solid black line*) and the PSF of the instrument (*dashed red line*), derived from Monte Carlo simulations. For all sources the reconstructed differential energy spectra are shown together with the best-fit power law (*solid line*).

#### 5.3.1. *HESS J1614−518*

This source (see Fig. 9) is located in a region relatively devoid of counterpart candidates. The source exhibits elliptical emission with a semimajor axis of $14' \pm 1'$ and a semiminor axis of $9' \pm 1'$. HESS J1614−518 is the brightest of the new sources, detected with a flux corresponding to 25% of that from the Crab Nebula above 200 GeV. The spectrum is well fitted by a power

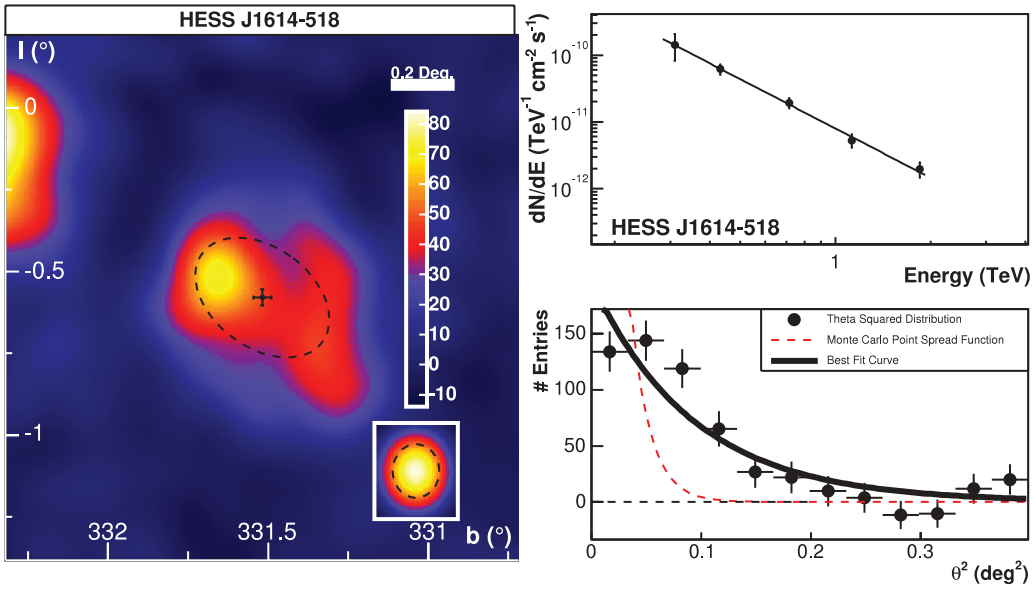


FIG. 9.—*Left*: Smoothed excess map (smoothing radius $0.^{\circ}09$) of the region of HESS J1614−518. *Right*: Energy spectrum (*top*) and $\theta^2$ plot (*bottom*).

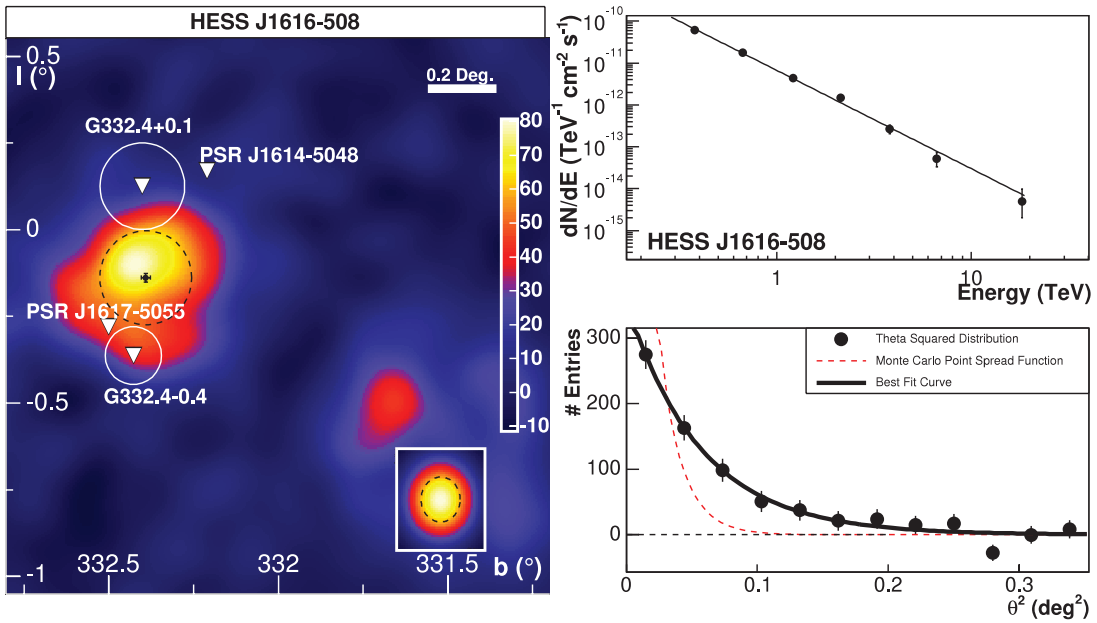


FIG. 10.—*Left*: Smoothed excess map (smoothing radius 0.°06) of the region surrounding HESS J1616−508 (*left-hand source*), along with nearby pulsars and SNRs that were considered as counterparts. HESS J1614−518 is also visible in this map (*right-hand source*). *Right*: Energy spectrum (*top*) and the radial distribution ($\theta^2$) plot (*bottom*).

law of photon index 2.46 ± 0.20 (see Fig. 9, *top right*). A nearby *Chandra* observation (Kastner et al. 2003) covered an area more than 10′ away from the best-fit position of HESS J1614−518 and showed no evidence for X-ray emission from the direction of the H.E.S.S. source. The poor quality of the fit to the radial distribution of HESS J1614−518 as is shown in Figure 9 (*bottom right*) indicates that the source is not well described by a symmetrical Gaussian profile.

### 5.3.2. *HESS J1616−508*

HESS J1616−508 (see Fig. 10), with a flux of 19% of the Crab Nebula above 200 GeV, is also one of the brighter new sources of VHE gamma rays. Its spectrum can be fitted by a power law of photon index 2.35 ± 0.06 as shown in Figure 10 (*top right*). The emission region has an rms size of 16′ and does not have a good positional match to any plausible counterpart at other wavelengths. It is located in a region close to the known SNRs G332.4−0.4 (RCW 103) and G332.4+0.1 (Kes 32). The region has been intensively studied with X-ray satellites like *Chandra* (Vink 2004) and *XMM-Newton*, with the position of HESS J1616−508 mostly outside or at the edge of the field of view where the sensitivity is strongly decreased. No extended X-ray source that lines up with the VHE gamma-ray emission has been found. Another interesting object in this region is the energetic pulsar PSR J1617−5055 (Torii et al. 1998), a young X-ray–emitting pulsar that was proposed to emit TeV gamma rays (Hirotani 2001). Approximately 1.2% of its spin-down luminosity would suffice to power the observed (0.2–10 TeV) VHE gamma-ray flux, assuming that the H.E.S.S. source is located at the pulsar distance. Since HESS J1616−508 does not line up with this object, an asymmetric (yet undetected) PWN powered by the pulsar would be required to explain the TeV emission.

### 5.3.3. *HESS J1632−478*

The centroid positions of this object (right-hand source in Fig. 11, *top*) and of the close-by HESS J1634−472 are spatially separated by less than 45′. HESS J1632−478 has an elongated shape with a semimajor axis of 12′ ± 3′ and a semiminor axis of 3.′6 ± 2.′4. Its flux in VHE gamma rays above 200 GeV corresponds to 12% of the flux from the Crab Nebula, and the spectrum can be fitted by a power law of photon index 2.12 ± 0.20 (see Fig. 11, *bottom right*). A positional coincidence of HESS J1632−478 exists with the hard X-ray source IGR J16320−4751 discovered by the *INTEGRAL* satellite (Tomsick et al. 2003) in the energy range above 15 keV. In softer X-rays between 2 and 10 keV, this object was also strongly detected in an *XMM-Newton* observation (Rodriguez et al. 2003) and found to be coincident with the *ASCA* source AX J1631.9−4752, detected in the *ASCA* Galactic plane survey (Sugizaki et al. 2001). This source is believed to belong to a new class of heavily absorbed high-mass X-ray binary systems, with an equivalent absorption column density of $(9.2 \pm 1.1) \times 10^{22}$ cm$^{-2}$ in this case. The extension of HESS J1632−478 does not plead in favor of an association with IGR J16320−4751. One should note that the probability of spurious associations is increased in this region of the Galactic plane (the 3 kpc arm tangent region) due to the high density of absorbed *INTEGRAL* sources. Another potential counterpart is the *ASCA* source AX J163252−4746.

### 5.3.4. *HESS J1634−472*

The size of the HESS J1634−472 (left-hand source in Fig. 11, *top*) emission region is 6.′6 ± 1.′8, and its flux above 200 GeV is close to 6% of the Crab flux with a photon index for the energy spectrum of 2.38 ± 0.26 (see Fig. 11, *middle left*). HESS J1634−472 has no direct positional counterpart, although it is interesting to note that yet another *INTEGRAL* source IGR J16358−4726 is located close by (Revnivtsev et al. 2003). This source presumably belongs to the class of highly absorbed X-ray binary systems, like IGR J16320−4751 (discussed in the previous paragraph). The source was detected in the 2–10 keV X-ray band with the *Chandra* satellite (Patel et al. 2004). The column density determined for this object is $N_{\rm H} = 3.3 \times 10^{23}$ cm$^{-2}$, and the luminosity of this object in the 2–10 keV band is $10^{36}$ ergs s$^{-1}$. Another potential counterpart of HESS J1634−472 is the recently discovered SNR

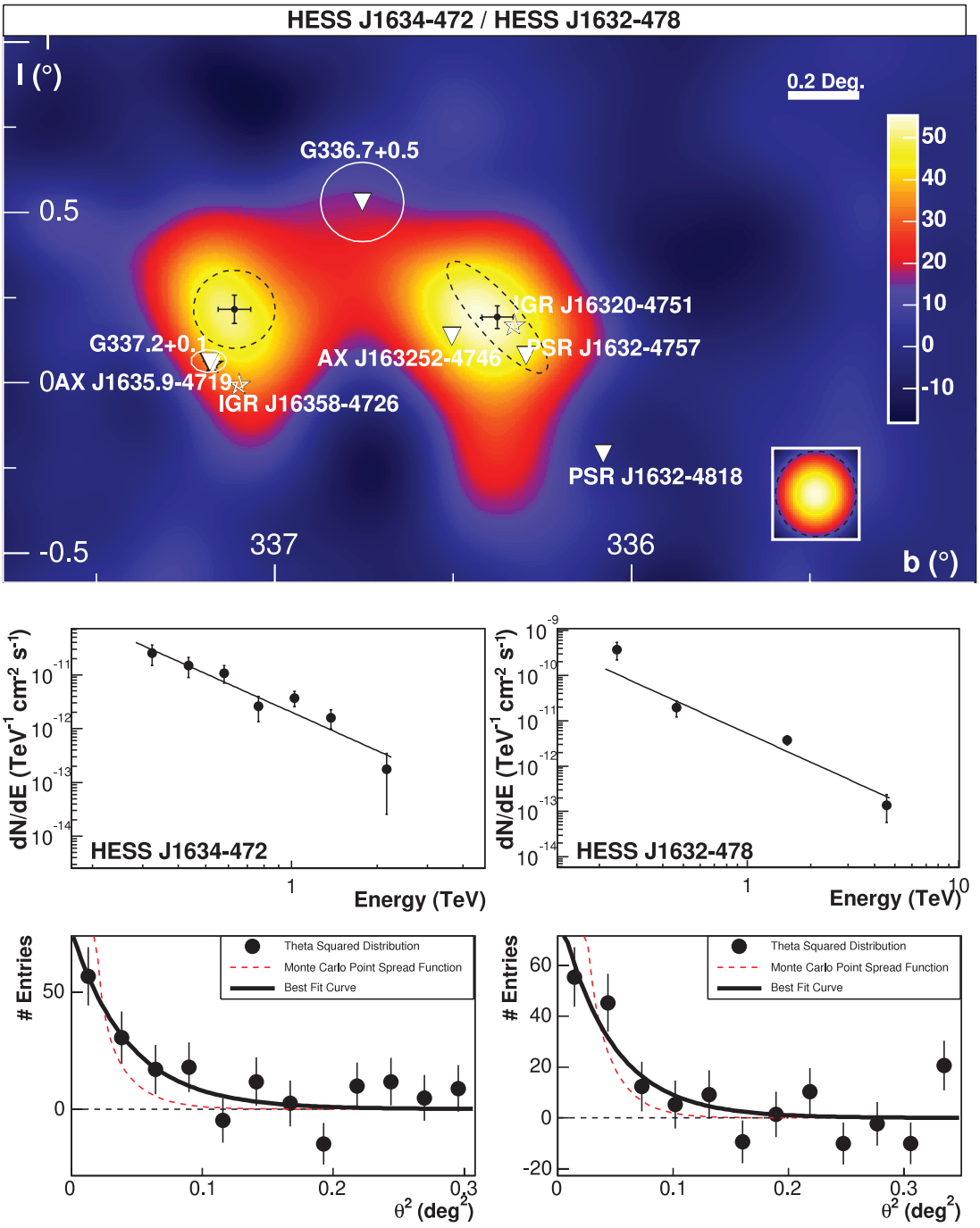


FIG. 11.—*Top*: Smoothed excess map (smoothing radius 0°.12) of the region of the two close-by H.E.S.S. sources HESS J1634−472 (*left-hand source*) and HESS J1632−478 (*right-hand source*), along with nearby pulsars, SNRs, and *INTEGRAL* sources that were considered as counterparts. It should be noted that the tail of HESS J1632−478 to negative Galactic latitude is statistically not significant. The panels in the middle row show the spectra (*left*: HESS J1634−472; *right*: HESS J1632−478), while the panels in the bottom row show the corresponding $\theta^2$ plots.

candidate G337.2+0.1 (Combi et al. 2005), coincident with the *ASCA* source AX J1635.9−4719. However, the distances of the two objects to HESS J1634−472 render a correlation unlikely.

### 5.3.5. *HESS J1640−465*

As can be seen from the radial distribution of this source (see Fig. 12, *bottom right*), HESS J1640−465 is marginally extended with respect to the PSF of the instrument. It is one of the few examples of an excellent spatial correlation between the VHE gamma-ray emission and an SNR (G338.3−0.0), known from radio observations (Green 2004). G338.3−0.0 was observed in the Molonglo Galactic plane survey at 843 MHz (shown in green contours in Fig. 12, *left*) and has been reported to be a broken shell SNR lying on the edge of a bright H II region (Whiteoak & Green 1996). The region bridging this SNR and the close-by SNR G338.5+0.1 is known to contain dense H II regions. The relation of surface brightness to distance yields a distance of 8.6 kpc, which would place the SNR in the 3 kpc arm tangent region. The *ASCA* source AX J164042−4632 with a photon index of $2.98^{+1.13}_{-0.89}$ and a flux level of $1.21 \times 10^{-12}$ ergs cm$^{-2}$ s$^{-1}$, detected during

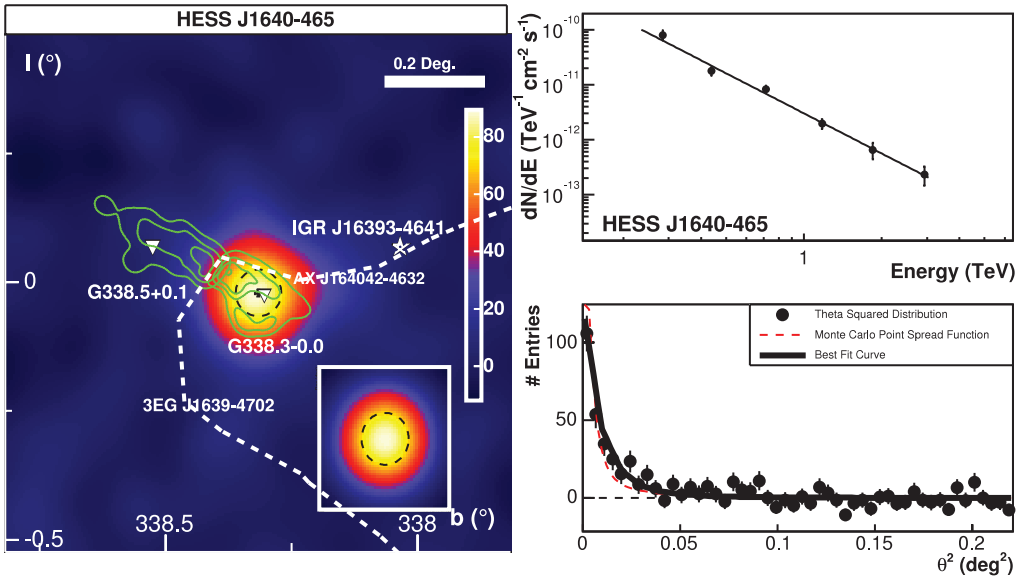


FIG. 12.—*Left*: Smoothed excess map (smoothing radius 0°.05) of the region surrounding HESS J1640−465 along with nearby SNRs that were considered as counterparts as discussed in the text. The green contours indicate the radio emission detected from the region surrounding G338.3−0.0 in the Molonglo Galactic plane survey at 843 MHz (Green et al. 1999). The dashed white contours show the 95% positional error of the unidentified EGRET source 3EG J1639−4702. *Right*: Differential energy spectrum (*top*) and the radial distribution ($\theta^2$) plot (*bottom*).

the *ASCA* Galactic plane survey (Sugizaki et al. 2001), has been identified with G338.3−0.0. It should be noted that the position of HESS J1640−465 is compatible with the position of the unidentified EGRET source 3EG J1639−4702 (Hartman et al. 1999). The 95% positional confidence contour of 3EG J1639−4702 is shown in Figure 12 (*left*). The distance of HESS J1640−465 to this EGRET source is 34′. The differential energy spectrum of HESS J1640−465 can be well fitted by a power law with photon index 2.42 ± 0.14 at a flux close to 9% of that from the Crab Nebula above 200 GeV (see Fig. 12, *top right*). A simple power-law extrapolation of the VHE gamma-ray spectrum to 1 GeV matches the EGRET flux above that energy.

### 5.3.6. *HESS J1702−420*

For HESS J1702−420 (Fig. 13) no significant evidence for extension of the emission region can be derived beyond a level of 2 standard deviations for the measured source size of 4.′8 ± 2.′4. The flux above 200 GeV of this source corresponds to 7% of the Crab flux, and the energy spectrum can be fitted by a power law of photon index 2.31 ± 0.15 (see Fig. 13, *top right*). The close-by pulsar PSR J1702−4128 is energetic enough to account for the observed VHE gamma-ray emission by converting roughly 14% of its spin-down luminosity but would need an asymmetric PWN to be responsible for the observed VHE gamma-ray

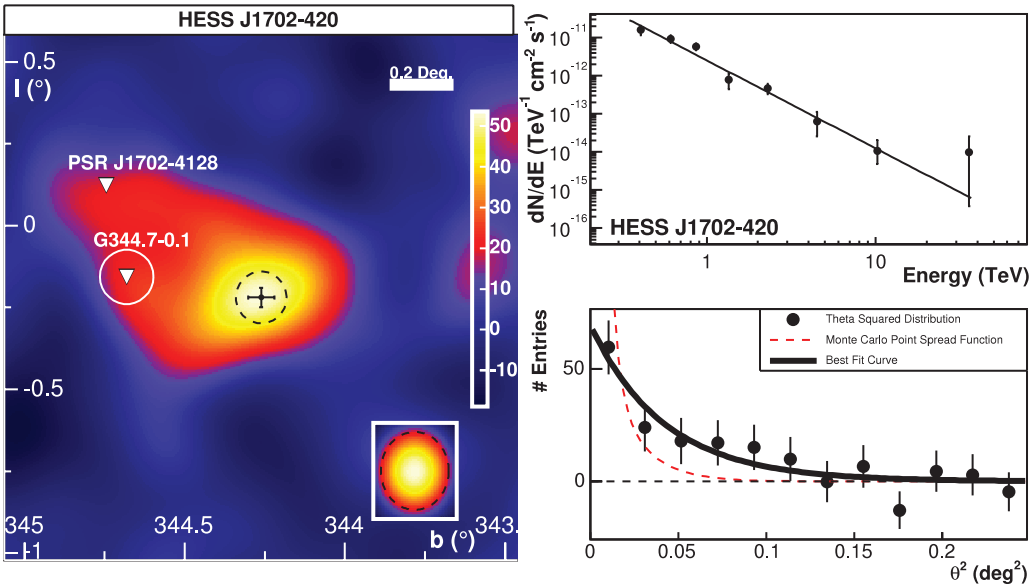


FIG. 13.—*Left*: Smoothed excess map (smoothing radius 0°.10) of the region surrounding HESS 1702−420 along with nearby pulsars and SNRs that were considered as counterparts as discussed in the text. The tail extending to positive Galactic longitude and latitude is not statistically significant. *Right*: Differential energy spectrum (*top*) and the radial distribution ($\theta^2$) plot (*bottom*).

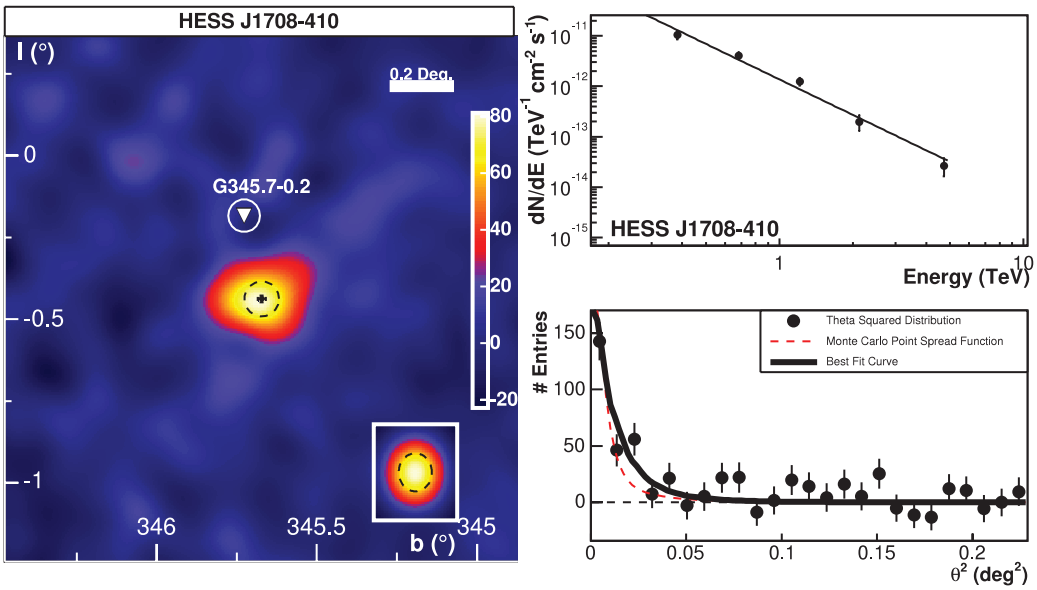


FIG. 14.—*Left*: Smoothed excess map (smoothing radius 0°.05) of the region surrounding HESS 1708−410 along with a nearby SNR that was considered as a counterpart. *Right*: Differential energy spectrum (*top*) and the radial distribution ($\theta^2$) plot (*bottom*).

emission. No asymmetric PWN has been detected from this pulsar, however, which renders an association unlikely. The nearby SNR G344.7−0.1 is too small and not positionally coincident with the VHE gamma-ray source. Therefore, we cannot identify a plausible counterpart for this object.

### 5.3.7. *HESS J1708−410*

This VHE gamma-ray source (Fig. 14) of size $3'.2 \pm 0'.7$ is located very close to SNR RX J1713.7−3946 and therefore its observation live time (within 2° of the pointing position of the instrument) amounts to 37.2 hr, well beyond typical exposures in the H.E.S.S. survey. The source exhibits an energy spectrum with a power-law index of $2.34 \pm 0.11$, and the flux above 200 GeV is less than 4% of the flux from the Crab Nebula (see Fig. 14, *top right*). As can be seen from Figure 14 (*left*), there is no close-by plausible counterpart. A nearby *XMM-Newton* observation of the SNR G345.7−0.2 has revealed no X-ray counterpart to the VHE gamma-ray source, but it should be noted that the offset of HESS J1708−410 from the center of the *XMM-Newton* field of view was 15′, positioning it close to the edge of the field of view. As can be seen from the radial distribution, shown in Figure 14 (*bottom right*), the source is only marginally extended with respect to the PSF of the instrument.

### 5.3.8. *HESS J1713−381*

This source (Fig. 15) is the second of the 14 VHE sources that show no significant evidence beyond 2 standard deviations for an extension of the emission region. The energy spectrum of HESS J1713−381 is consistent with a power law with photon index $2.2 \pm 0.5$. Its flux of 1.8% of the flux from the Crab Nebula above 200 GeV makes this object the weakest of the new sources. Its location is very close to the strong VHE gamma-ray source SNR RX J1713.7−3946, and it was therefore in the field of view of most pointed observations by H.E.S.S. on this object. The correspondingly deep exposure of 37 hr at offsets of less than 2° from the center of the field of view made it possible to detect this object. As can be seen from Figure 15 (*left*), it coincides with part of the unusual SNR complex CTB 37. The radio contours of the CTB 37 complex as taken from the Molonglo Galactic plane survey at 843 MHz are shown in white (Green et al. 1999). There is clear positional match between the source HESS J1713−381 and the SNR G348.7+0.3 (CTB 37B). Also visible in Figure 15 (*right*) is a weaker marginal source consistent with the position of G348.5+0.1 (CTB 37 A). The marginal detection of emission from this source is however not significant after accounting for all trials for the analysis of extended sources in this survey as described above. Kassim et al. (1991) describe CTB 37A as two SNRs overlapping in projection: with the partial shell of G348.7+0.1 in the west and the SNR G348.5−0.0 to the east. Both SNRs in CTB 37A appear to be interacting with a system of molecular clouds with densities of 100–1000 $cm^{-3}$ (Reynoso & Mangum 2000). The SNR CTB 37B is less well studied but appears to share the dense environment of CTB 37A. Evidence for X-ray emission from the CTB 37 complex can also be seen in archival *ASCA* data.

### 5.3.9. *HESS J1745−303*

This object (Fig. 16) has a direct positional coincidence with an unidentified EGRET source (3EG J1744−3011; Hartman et al. 1999). Since it is within the field of view of the Galactic center, HESS J1745−303 has a large observation live time of 35.3 hr. Its flux level corresponds to 5% of the flux from the Crab Nebula above 200 GeV, and the emission exhibits a hard differential flux of index $1.8 \pm 0.3$. Its emission region has an elliptical shape with a semimajor axis of $13' \pm 4'$ and a semiminor axis of $5'.4 \pm 2'.4$ as is shown in Figure 16 (*left*). The distance of HESS J1745−303 to the centroid of the EGRET source 3EG J1744−3011 is 10′, which is well within the 95% uncertainty level of the EGRET position. A simple power-law extrapolation of the VHE gamma-ray spectrum to energies above 1 GeV is an order of magnitude below the EGRET flux above that energy [$F(>100\ \mathrm{MeV}) = (64 \pm 7) \times 10^{-8}\ \mathrm{cm}^{-2}\ \mathrm{s}^{-1}$]. Another potential counterpart is the pulsar PSR B1742−30, but essentially 100% of its spin-down power would be required to account for the entire VHE gamma-ray emission.

### 5.3.10. *HESS J1804−216*

This source (Fig. 17), with a size of approximately 22′, is the largest of the new emission regions of VHE gamma rays.

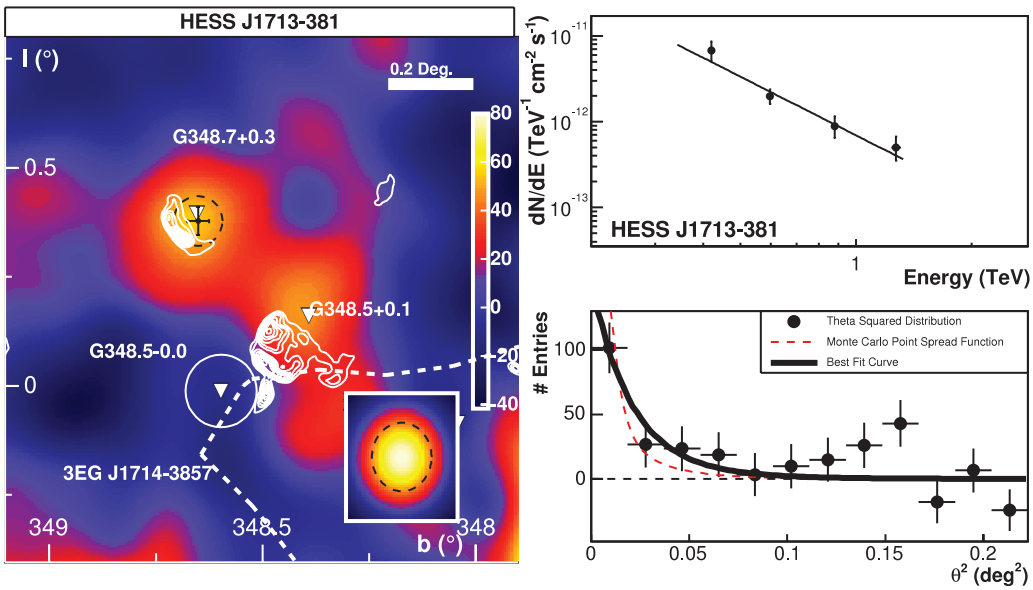


FIG. 15.—*Left*: Smoothed excess map (smoothing radius 0.°07) of the region surrounding HESS J1713−381 along with nearby SNRs that were considered as counterparts as discussed in the text. In the lower right corner of this excess map, the strong VHE emission from SNR RX J1713.7−3946 is apparent. The white contours show the radio emission as seen in the Molonglo plane survey at 843 MHz (Green et al. 1999). The marginal excess in positional agreement with G348.5+0.1 (CTB 37A) is not significant after accounting for all trials for the analysis presented here. *Right*: Differential energy spectrum (*top*) and the radial distribution ($\theta^2$) plot (*bottom*). Also in the radial distribution, some indication for an excess ∼0.°4 away from HESS J1713−381 can be seen, due to the marginal excess at the position of CTB 37A. The dashed white contours show the 95% positional error of the unidentified EGRET source 3EG J1714−3857.

With a flux of nearly 25% of the flux from the Crab Nebula above 200 GeV, it is also the brightest of the new H.E.S.S. sources. The photon index of 2.72 ± 0.06 makes it one of the softest sources (see Fig. 17, *top right*). As can be seen from Figure 17 (*left*), the emission region does not perfectly line up with any known object, although it could be associated with the southwestern part of the shell of the SNR G8.7−0.1 of radius 26′. From CO observations, the surrounding region is known to be associated with molecular gas where massive star formation takes place (Ojeda-May et al. 2002). The white contours in Figure 17 (*left*) show soft X-ray emission as detected by the *ROSAT* satellite (Finley & Ögelman 1994), while the black contours show the 20 cm radio emission as recorded with the VLA. Another plausible association of HESS J1804−216 is the young Vela-like pulsar PSR J1803−2137 with a spin-down age of 16,000 yr (Kassim & Weiler 1990). The required efficiency of this pulsar's spin-down luminosity to power the observed emission in gamma rays is only 3%, and it could therefore easily account for the new source.

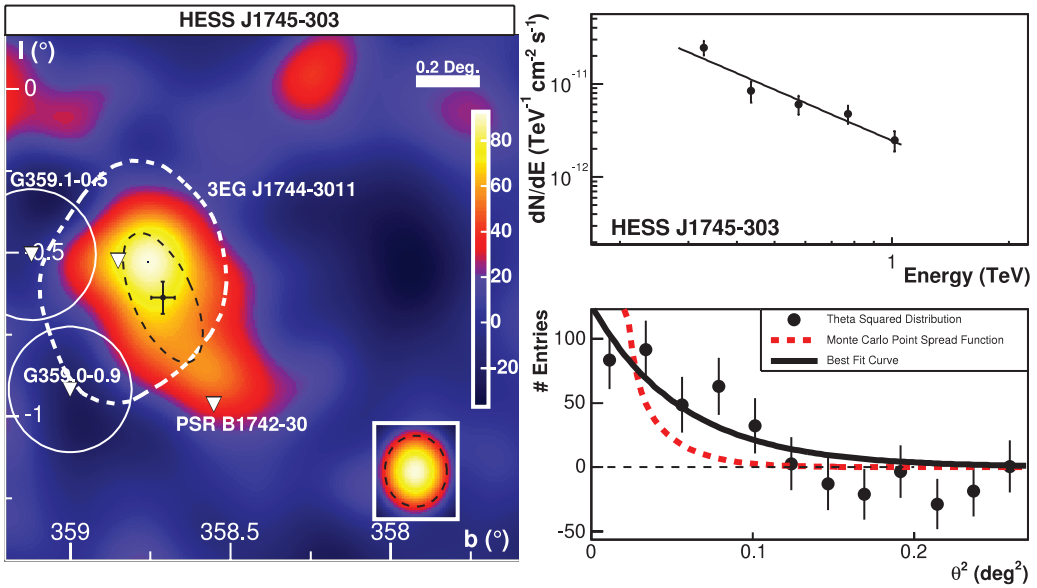


FIG. 16.—*Left*: Smoothed excess map (smoothing radius 0.°10) of the region surrounding HESS J1745−303 along with nearby pulsars and SNRs that were considered as counterparts as discussed in the text. *Right*: Differential energy spectrum (*top*) and the radial distribution ($\theta^2$) plot (*bottom*).

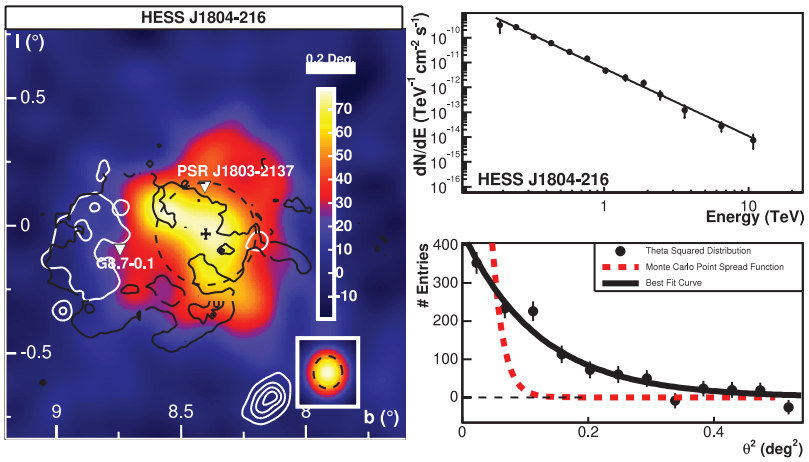


FIG. 17.—*Left*: Smoothed excess map (smoothing radius 0.°06) of the region surrounding HESS J1804−216 along with nearby pulsars and SNRs that were considered as counterparts as discussed in the text. The white contours show the X-ray emission from G8.7−0.1 as detected by the *ROSAT* satellite, while the black contours show the 20 cm radio emission detected by the VLA. *Right*: Differential energy spectrum (*top*) and the radial distribution ($\theta^2$) plot (*bottom*).

### 5.3.11. *HESS J1813−178*

With a moderate flux of approximately 6% of the Crab Nebula above 200 GeV, this source (see Fig. 18) is among the more compact of the new sources with an extension of 2.′2. When using a large $\theta^2$ cut of $(0.°4)^2$, the normalization of the power-law fit is 25% higher, suggesting a faint non-Gaussian tail in the radial brightness profile. The source exhibits a rather hard photon index of $2.09 \pm 0.08$ (see Fig. 18, *top right*). In the previous publication (Aharonian et al. 2005f) this source was still considered as unidentified. As it is clear from Figure 18 (*left*), there is a compelling positional coincidence between this source and the X-ray source AX J1813−178 (Brogan et al. 2005) (shown by white contours in Fig. 18 for the 0.7–10 keV band). This *ASCA* source is one of the bright sources detected in the *ASCA* Galactic plane survey with a very hard energy spectrum. This object was also recently detected in the *INTEGRAL* Galactic plane survey in the 20–100 keV energy band (Ubertini et al. 2005). The region surrounding HESS J1813−178 was also observed with the VLA, and 20 cm radio contours are shown in black in Figure 18. There is a faint radio source (G12.82−0.02) with a shell-like structure visible at the position of HESS J1813−178 as also recently reported (Brogan et al. 2005; Helfand et al. 2005). This indicates a probable association with a shell-type SNR. Additionally HESS J1813−178 lies 10′ from the center of the radio source W33. W33 extends over 15′ and has a compact radio core (G12.8−0.2) that is 1′ across (Haschick & Ho 1983), located ∼15′ away from HESS J1813−178. The W33 region shows signature of an ultracompact

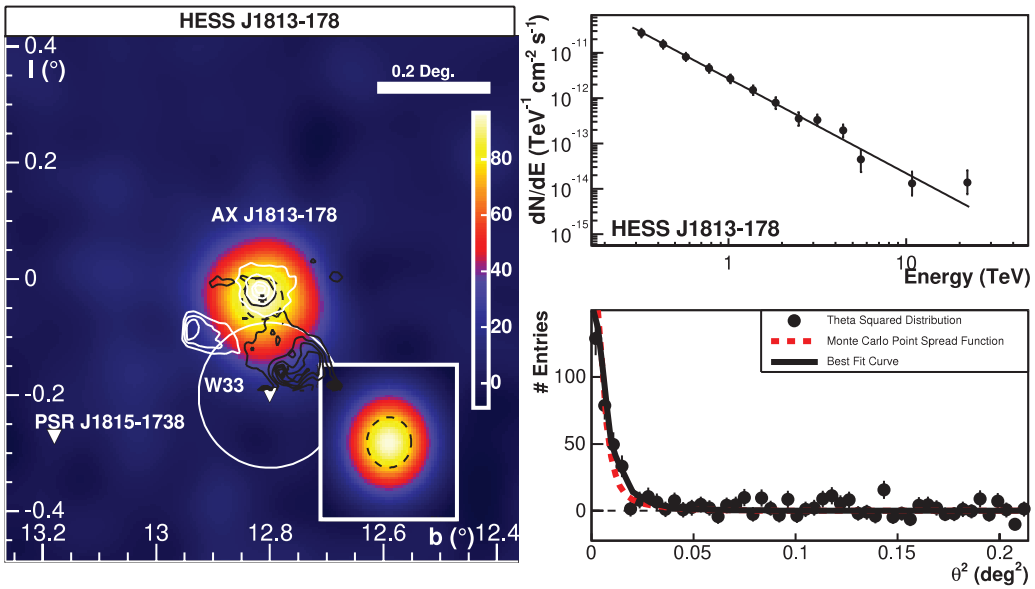


FIG. 18.—*Left*: Smoothed excess map (smoothing radius 0.°04) of the region surrounding HESS J1813−178 along with nearby pulsars and SNRs that were considered as counterparts as discussed in the text. The white contours show the smoothed X-ray count map for the region surrounding AX J1813−178 obtained by *ASCA* with the GIS instrument in the 0.7–10 keV band, while the black contours show 20 cm radio emission as observed by the VLA. The strong radio source to negative Galactic longitudes from HESS J1813−178 is connected to the W33 complex and extends farther than shown here. The excess seen to negative Galactic longitudes at the edge of the ASCA GIS field of view is likely due to contamination from GX 13+1. The radial (*bottom right*) distribution ($\theta^2$) plot shows that the source is marginally extended with respect to the PSF of the H.E.S.S. system.

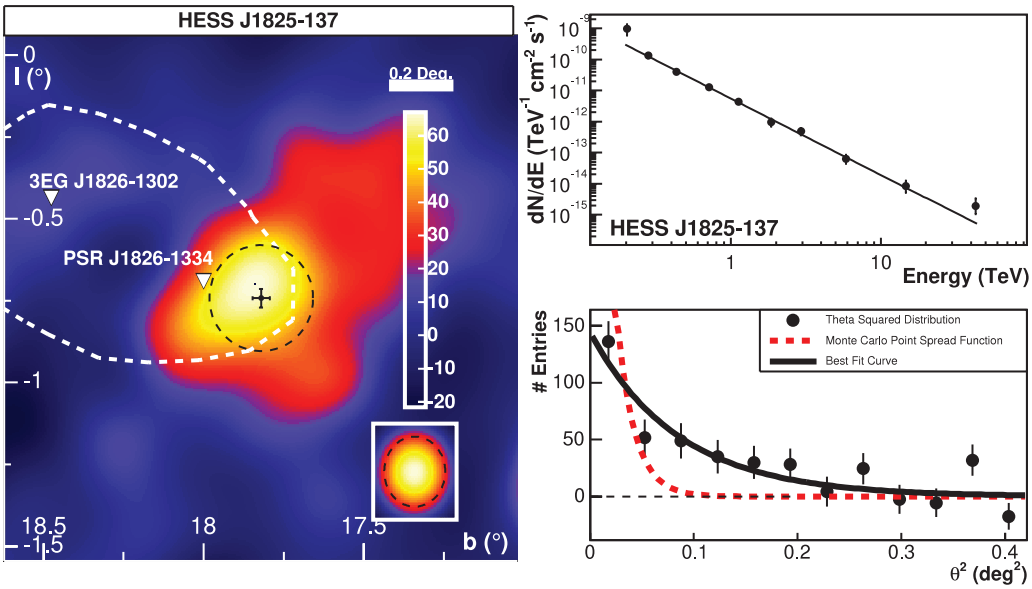


FIG. 19.—*Left*: Smoothed excess map (smoothing radius 0.°09) of the region surrounding HESS J1825−137 along with the nearby pulsar that was considered as a counterpart as discussed in the text. *Right*: Differential energy spectrum (*top*) and the radial distribution ($\theta^2$) plot (*bottom*).

H II region (Churchwell 1990) and contains methanol, hydroxyl, and water masers and other tracers of recent star formation, which could act as target material for the generation of VHE gamma rays but is not coincident with the H.E.S.S. source.

### 5.3.12. *HESS J1825−137*

This source has an energy spectrum with a photon index of $2.46 \pm 0.08$ and a flux of VHE gamma rays of approximately 17% of the flux from the Crab Nebula above 200 GeV (see Fig. 19, *top right*). It is approximately radially symmetric, and the emission region can be best described by a Gaussian of width 10′. The position of HESS J1825−137 is approximately 11′ to negative Galactic longitudes of the young pulsar PSR B1823−13 (PSR J1826−1334), which makes an association of the VHE gamma-ray source with the pulsar possible. The pulsar PSR B1823−13 is a 101 ms evolved Vela-like pulsar at a distance of $3.9 \pm 0.4$ kpc, and at this distance the VHE luminosity of HESS J1825−137 would only be ∼2% of its spin-down power. The region surrounding the pulsar has been previously observed at large zenith angles by the Whipple collaboration (Hall et al. 2003), who observed a 3.1 $\sigma$ excess also to negative Galactic longitudes with respect to the pulsar position. X-ray observations with the *XMM-Newton* satellite show a 5′ diameter diffuse emission region extending also asymmetrically to negative Galactic longitudes from the pulsar (Gaensler et al. 2003). If the VHE gamma-ray source is indeed associated with this PWN, the VHE emission region would

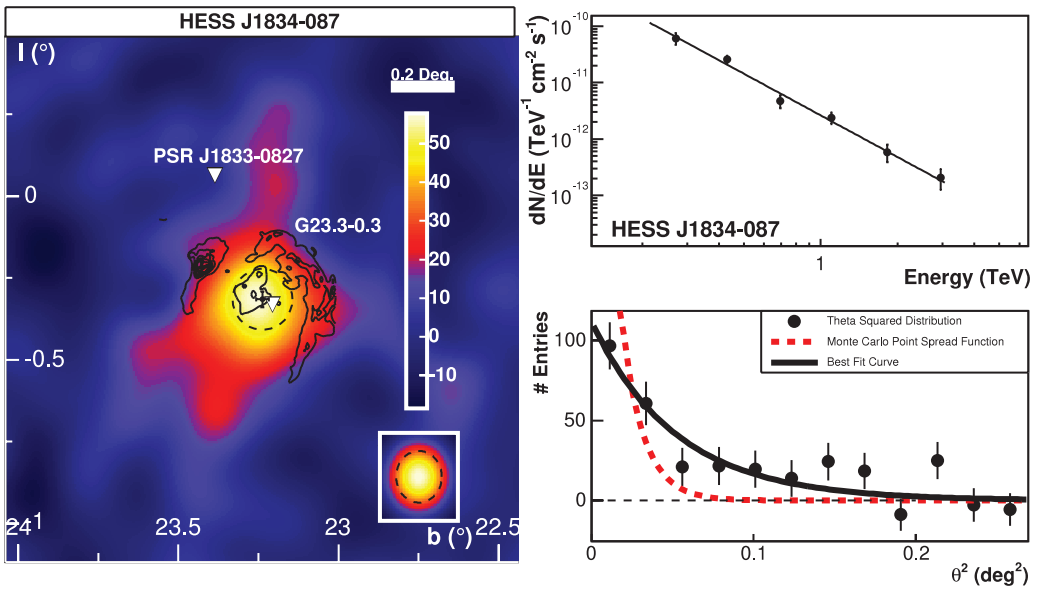


FIG. 20.—*Left*: Smoothed excess map (smoothing radius 0.°08) of the region surrounding HESS J1834−087 along with nearby pulsars and SNRs that were considered as counterparts as discussed in the text. The positional coincidence with SNR G23.3−0.3 (W41) is evident; the black contours show 20 cm radio emission recorded by the VLA (White et al. 2005). *Right*: Differential energy spectrum (*top*) and the radial distribution ($\theta^2$) plot (*bottom*).

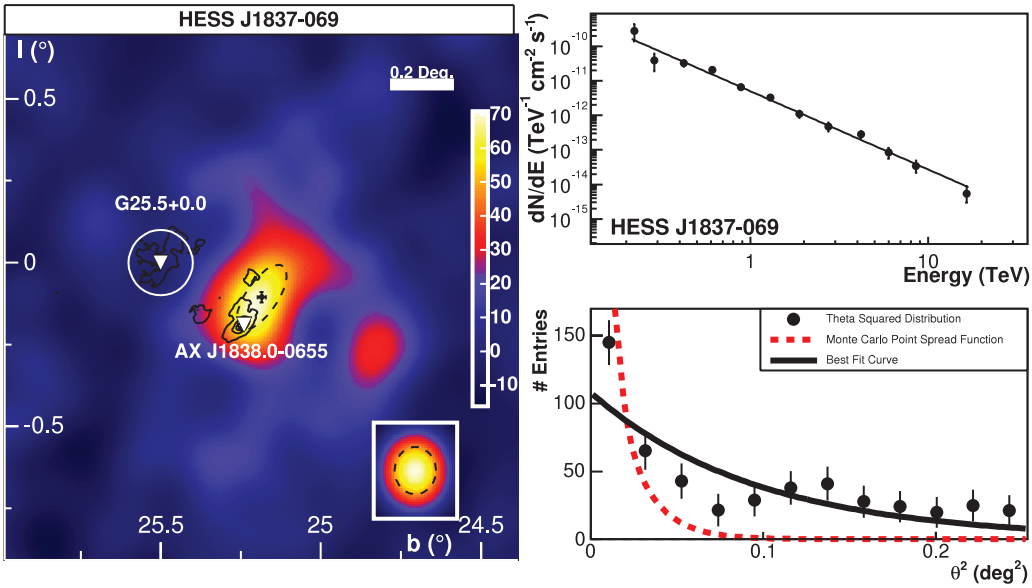


FIG. 21.—*Left*: Smoothed excess map (smoothing radius 0°.05) of the region surrounding HESS J1837−069 along with nearby SNRs that were considered as counterparts as discussed in the text. The black contours show the smoothed X-ray count map for the region surrounding AX J1838.0−0655 obtained by *ASCA* with the GIS instrument in the 0.7–10 keV band. The positional coincidence of HESS J1836−069 with the *ASCA* source AX J1838.0−0655 is evident. *Right*: Differential energy spectrum (*top*) and the radial distribution ($\theta^2$) plot (*bottom*).

extend much farther to the south than in X-rays. PSR B1823−13 was also proposed to power the close-by unidentified EGRET source 3EG J1826−1302 (Nolan et al. 2003). The distance of the centroid of this EGRET source to HESS J1825−137 is 43′. As illustrated in Figure 19 (*left*), the new VHE gamma-ray source is well compatible with the EGRET source within the 95% positional error of EGRET, and a simple power-law extrapolation of the H.E.S.S. energy spectrum to energies above 1 GeV gives a similar flux as derived from the EGRET spectrum above this energy. An in-depth study of HESS J1825−137 and discussion about the corresponding PWN model will be given in a separate paper (Aharonian et al. 2005e).

#### 5.3.13. *HESS J1834−087*

HESS J1834−087 (Fig. 20) has a size of 12′ and a gamma-ray flux of 8% of the flux from the Crab Nebula above 200 GeV. Its energy spectrum exhibits a photon index of 2.45 ± 0.16 (see Fig. 20, *top right*). When using a large $\theta^2$ cut of $(0.^\circ4)^2$, the normalization of the power-law fit increases by 30%, suggesting a deviation of the morphology from the assumed radial Gaussian brightness profile. The location of HESS J1834−087 makes it another source with a compelling positional agreement with an SNR (see Fig. 20, *left*). The positionally coincident shell-type SNR G23.3−0.3 (W41) with a diameter of 27′ was mapped in radio with the VLA at 330 MHz (Kassim 1992) and at 20 cm (White et al. 2005) as shown in black contours in Figure 20 (*left*). It is possibly connected to the old pulsar PSR J1833−0827 (Gaensler & Johnston 1995). This pulsar is energetic enough to power HESS J1834−087, but its distance of 24′ renders an association unlikely; there is also no extended PWN detected so far.

#### 5.3.14. *HESS J1837−069*

This source (Fig. 21) has an elongated shape with a semimajor axis of 7′ ± 1′ and a semiminor axis of 3′ ± 1′. With a flux of 13.4% of the Crab flux above 200 GeV, the energy spectrum can be well fitted by a power law of photon index 2.27 ± 0.06 (see Fig. 21, *top right*). When using a large $\theta^2$ cut of $(0.^\circ4)^2$, the normalization of the power-law fit increases by 30%, suggesting that the assumption of a Gaussian brightness profile does not hold for this source. HESS J1837−069 coincides with the southern part of the diffuse hard X-ray complex G25.5+0.0. This source, which is 12′ across, was detected in the *ASCA* Galactic plane survey (Bamba et al. 2003). The nature of this bright X-ray source is unclear, but it may be an X-ray synchrotron emission dominated SNR such as SN 1006 or a PWN. The brightest feature in the *ASCA* map (AX J1838.0−0655), located south of G25.5+0.0, coincides with the VHE emission. This still unidentified source was also serendipitously detected by *BeppoSAX* and also in the hard X-ray (20–100 keV) band in the Galactic plane survey of *INTEGRAL* (Malizia et al. 2004).

## 6. DISCUSSION

Possible multiwavelength associations of the 14 new VHE gamma-ray sources were discussed in the previous section and are summarized in Table 5. A further qualification from tentative associations to unambiguous counterpart identifications requires spatial or morphological coincidence, a viable gamma-ray emission mechanism for the object, and consistent multiwavelength behavior according to the properties of the suggested identification. Most of the possible associations given above can be considered as plausible gamma-ray emitters, but only in a minority of these cases does a satisfactory positional coincidence exist. Four of the new sources apparently line up with SNRs. These SNRs have been detected and studied mostly in the radio domain, but in the cases of HESS J1640−465 and HESS J1813−178 X-ray emission was detected by *ASCA*, and there is marginal evidence for X-ray emission in *ASCA* archival data in the case of HESS J1713−381. Only in the case of HESS J1834−087 is there currently no evidence for associated X-ray emission.

For three of the new sources, namely, HESS J1616−509, HESS J1804−216, and HESS J1825−137, a sufficiently energetic nearby pulsar could account for the VHE gamma-ray emission,

TABLE 5
SUMMARY OF POSSIBLE COUNTERPARTS TO THE H.E.S.S. VHE GAMMA-RAY SOURCES IN THE INNER GALAXY

| Name | Possible Counterpart | Class | Offset (arcmin) | Distance (kpc) | Luminosity ($10^{34}$ ergs $s^{-1}$) |
|---|---|---|---|---|---|
| J1614−518 | ... | ... | ... | ... | ... |
| J1616−508 | PSR J1617−5055 | PWN | 10.4 | 6.5 | 20.2 |
| J1632−478 | IGR J16320−4751 | XRB | 3 | ... | ... |
| J1634−472 | IGR J16358−4726/G337.2+0.1 | XRB/SNR | 13/10 | .../14 | .../28.3 |
| J1640−465 | G338.3−0.0/3EG J1639−4702 | SNR/UID | 0/34 | 8.6 | 16.2 |
| J1702−420 | ... | ... | ... | ... | ... |
| J1708−410 | ... | ... | ... | ... | ... |
| J1713−381 | G348.7+0.3 | SNR | 0 | 10.2 | 5.2 |
| J1713−397 | RX J1713.7−3946 (G347.3−0.5) | SNR | 0 | 1 | 1.2 |
| J1745−290 | Sgr A East/Sgr A* | SNR/BH | 0 | 8.5 | 12.8 |
| J1745−303 | 3EG J1744−3011 | UID | 10 | ... | ... |
| J1747−281 | G0.9+0.1 | PWN | 0 | 8.5 | 4.4 |
| J1804−216 | G8.7−0.1/PSR J1803−2137 | SNR/PWN | 21/10.8 | 6/3.9 | 16.5/7.0 |
| J1813−178 | G12.82−0.02 | SNR | 0 | 4 | 3.1 |
| J1825−137 | PSR J1826−1334/3EG J1826−1302 | PWN/UID | 11/43 | 3.9/... | 6.1/... |
| J1834−087 | G23.3−0.3 | SNR | 0 | 4.8 | 4.4 |
| J1837−069 | AX J1838.0−0655 | UID | 6 | ... | ... |

NOTES.—The offset denotes the angular distance of the VHE gamma-ray source from the possible counterpart. Distances are taken from Green (2004), Manchester et al. (2005), and references therein. The last column gives the implied luminosity between 0.2 and 10 TeV. The three sources that were known before the H.E.S.S. survey in the inner Galaxy (HESS J1747−218, HESS J1745−290, and HESS J1713−397) have been added for completeness to this table. The possible source classes have been abbreviated according to the following scheme: supernova remnant (SNR), unidentified sources (UID), pulsar wind nebula (PWN), black hole candidate (BH), X-ray binaries (XRB).

but the offset of the sources from the pulsar positions makes these associations less firm. Three of the new VHE gamma-ray sources are consistent with the 95% positional error of unidentified EGRET sources (HESS J1640−465, HESS J1745−303, and HESS J1825−137). Two of the new sources are located very close to a new class of highly absorbed hard X-ray sources detected recently by *INTEGRAL* (HESS J1632−478 and HESS J1634−472). A third source (HESS J1837−067) may be related to X-ray emission of unknown origin detected by *ASCA* and *INTEGRAL*, which may belong to the same class of objects. The three remaining sources (HESS J1614−518, HESS J1702−420, and HESS J1708−410) have no plausible SNR, pulsar, or EGRET counterpart and may belong to a new source class. Significant fluxes of VHE gamma rays without accompanying X-ray and radio emission would suggest the absence of relativistic electrons and the presence of energetic nucleons. That such a population exists is already being suggested by the detection of apparently "dark" accelerators by the HEGRA (Aharonian et al. 2002a) and H.E.S.S. (Aharonian et al. 2005d) collaborations. However, the possibility remains that these new sources are associated with SNRs or PWNs as yet undiscovered at other wavelengths. Further multiwavelength investigations are needed to clarify this picture.

The nearest energy band relative to the H.E.S.S. energy range was covered by observations with EGRET aboard the *Compton Gamma Ray Observatory*. Its energy coverage was primarily between 30 MeV and 10 GeV, and gamma-ray source detections above 100 MeV resulted in the third EGRET (3EG) catalog (Hartman et al. 1999). The only Galactic sources detected above 10 GeV are pulsars, for which the sparse photons at these energies correlate with the location and the pulse profile at lower EGRET energies (Thompson et al. 2005). The bulk of photons above 10 GeV have to be attributed to Galactic (and extragalactic) diffuse emission.

When comparing the EGRET sources with the H.E.S.S. Galactic plane survey result, it should be noted that even if an EGRET source spectrum is measured up to 10 GeV, more than a decade in energy is left uncovered below the H.E.S.S. energy threshold. Indeed, only a minor fraction of the H.E.S.S. sources coincide within the considerably larger location uncertainty contours of EGRET sources. These sources are HESS J1640−465, HESS J1745−303, and HESS J1825−137, which are consistent with the 95% location uncertainty of the unidentified EGRET sources 3EG J1639−4702, 3EG J1744−3011, and 3EG J1826−1302. In total 17 EGRET sources are cataloged within the H.E.S.S. survey region. Taking into account the 95% positional error contours, they cover an area of 9.76 $deg^2$, resulting in a chance positional coincidence of a given H.E.S.S. source with an EGRET source of 32%. A correlated Galactic latitude distribution of the EGRET and H.E.S.S. sources, concentrated near the Galactic plane, could increase this probability.

Physical arguments suggest that the EGRET source population and the set of new H.E.S.S. sources might be of different kinds. While the brightest gamma-ray pulsars can be directly traced up to ~20 GeV, EGRET data indicate the existence of GeV cutoffs already in the 2–10 GeV range (Reimer & Bertsch 2001). The brightest pulsars and several unidentified EGRET sources with pulsar-like characteristics deviate from single power-law spectral representations (Bertsch et al. 2000) and are significantly better fitted when introducing high-energy spectral cutoffs. GeV cutoffs are indeed predicted from multifrequency modeling of the gamma-ray emission of pulsars (Cheng 2004; Baring 2004). Therefore, the emission of these unidentified EGRET sources may not extend up to the H.E.S.S. energy range. From Crab measurements by CELESTE (de Naurois et al. 2002), consecutively continuing the EGRET GeV data, a characteristic change in the emission properties of the pulsar became apparent: pulsed emission is diminished or entirely absent, leaving only a steady emission component, in the case of Crab attributed to the PWN. If the majority of EGRET sources in the Galactic plane may be identifiable with gamma-ray pulsars, this population will overlap with the H.E.S.S. energies only if plerionic emission components exist.

For PWNs there are theoretical grounds to expect in some cases a displacement of the gamma-ray emission from the pulsar powering the nebula (Aharonian et al. 1997a; Blondin et al. 2001).

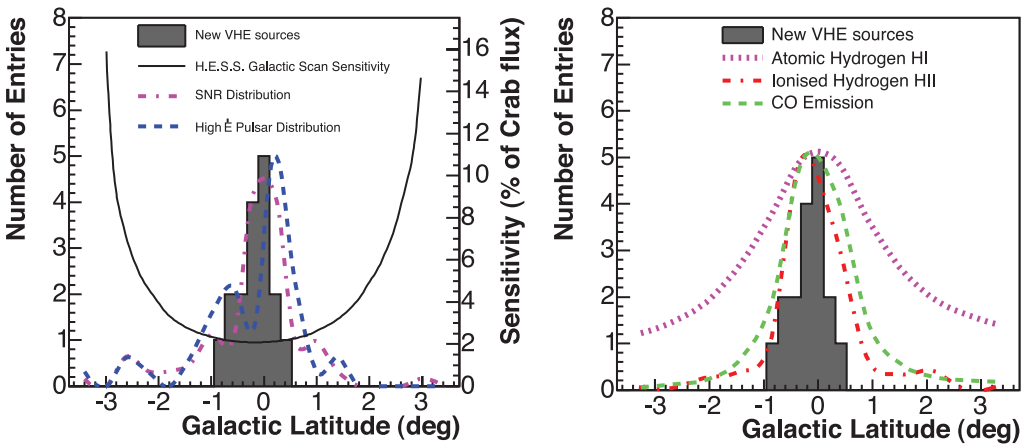


FIG. 22.—Distribution of Galactic latitude of the 17 VHE gamma-ray sources as given in Table 5 (the 14 new plus the 3 previously known). The mean of the distribution is −0.17 with an rms of 0.31. On the left, the distribution is shown along with the distribution in Galactic latitude of possible counterpart populations to the VHE gamma-ray sources. SNRs from Green (2004) are shown by a dot-dashed purple line, while high spin-down luminosity pulsars ($\dot{E} > 10^{34}$ ergs s$^{-1}$) taken from the ATNF catalog (Manchester et al. 2005) are shown by a dashed blue line. On the right, the distribution of VHE gamma-ray sources as on the left is shown along with the latitude distributions of matter in our Galaxy. The distribution of molecular hydrogen (H II; Paladini et al. 2003) is shown by a dot-dashed red line, the distribution of atomic hydrogen (H I; Dickey & Lockman 1990) is shown by a dotted purple line, and the distribution of CO (Dame et al. 2001) is shown by a dashed green line.

In such cases the association becomes more difficult to establish. Considering only pulsars with sufficient spin-down luminosity to explain the measured VHE gamma-ray flux, four of the new sources have possible associations with PWNs. However, only in the case of HESS J1825−137 is there so far a convincing multiwavelength argument for the offset from the pulsar position in the sense that an X-ray PWN offset in the source direction has been detected.

The sensitivity shown in Figure 3 is that for pointlike ($<0.^\circ1$) sources. The sensitivity of H.E.S.S. decreases with increasing source size: $F_{\rm min} \sim F_{\rm point\text{-}source}(\sigma^2_{\rm source} + \sigma^2_{\rm PSF})^{1/2}/\sigma_{\rm PSF}$, where $\sigma_{\rm PSF} \sim 0.^\circ08$ for the analysis described here. As a consequence, there is a bias in this survey against very extended sources. In particular, for sources larger than the size of the ring used for background estimation ($0.^\circ6$ radius) the flux threshold increases dramatically since the off-source region used for the background estimation then also contains flux from the source. This effect also introduces a bias against close-by sources, potentially resulting in a latitude distribution narrower than that of the parent population. An additional consequence of the ring background technique is that this survey is insensitive to weak diffuse emission. A search for diffuse emission in this data set will be reported elsewhere. Another effect that has an impact on the width of the latitude distribution is source confusion. Assuming that all sources lie on the Galactic plane and using the mean rms size of $0.^\circ1$ of the new sources, the chance probability of an overlap between any 2 of the 17 sources in the scan region is estimated to be 6%. Therefore, while source confusion could in principle widen the observed latitude distribution, we expect this effect to be small.

It is apparent from Table 5 that the most likely associations of the gamma-ray sources lie at rather large distances (i.e., 4–10 kpc) within our Galaxy and exhibit luminosities in the range $(3–20) \times 10^{34}$ ergs s$^{-1}$. Three of the new sources are located in a region of the Galactic plane that lines up with the 3 kpc arm tangent region (HESS J1640−465, HESS J1632−478, and HESS J1634−472), which hints at a distance of 8 kpc. HESS J1614−518 and HESS J1616−508 are at a position in the plane that lines up with the Norma spiral arm. This arm appears to be one of the most important massive star forming regions of the Galaxy (Bronfman et al. 2000).

As is clear from Table 5, it is difficult to explain the new VHE sources as belonging to a single source population. It is therefore not straightforward to interpret the global properties of the sources. However, conventional Galactic particle accelerators such as young pulsars and SNRs have similar spatial distribution within the Galaxy. Molecular material and hence regions of star formation cluster rather close to the Galactic plane, with an exponential scale height of <100 pc (Dame & Thaddeus 1994). Gamma-ray sources associated with stellar death (and birth) (SNRs, young pulsars, OB associations) should therefore follow similar distributions (see Fig. 22). To compare such candidate populations with the observed Galactic latitude distribution of the survey sources, assumptions must be made about the luminosity distribution, the radial distribution in the Galaxy, and the intrinsic size of the sources. A simple Monte Carlo simulation shows that the measured $b$ distribution of sources is rather insensitive to the assumed luminosity distribution.

Taking the example case of SNRs as being a single class of counterparts to the new sources, it is possible to derive the expected properties of the detected gamma-ray sources. For this exercise, the prescription of Drury et al. (1994) as given in equation (1) is followed for the gamma-ray emission of SNRs assuming supernova explosions with fixed energy $10^{51}$ ergs s$^{-1}$ occurring at a rate of 1/40 yr$^{-1}$ and with a gamma-ray–emitting lifetime of $10^4$ yr. In this case, 250 gamma-ray sources are expected within the Galactic disk. Assuming the radial distribution of SNRs suggested by Case & Bhattacharya (1996), the measured number of the VHE gamma-ray sources is consistent with expectations for plausible values of conversion efficiency into accelerated particles $\Theta = 0.2$ and ISM density $n = 1$ cm$^{-3}$. As the sensitivity of the survey is reduced for extended sources, some assumption of the intrinsic size distribution of sources must be made. Here the Sedov solution is assumed to determine the size of the gamma-ray emission region for an SNR, of randomly sampled age, expanding into an ISM of density $n$. Reasonable agreement with the number and angular size of the detected sources is found for

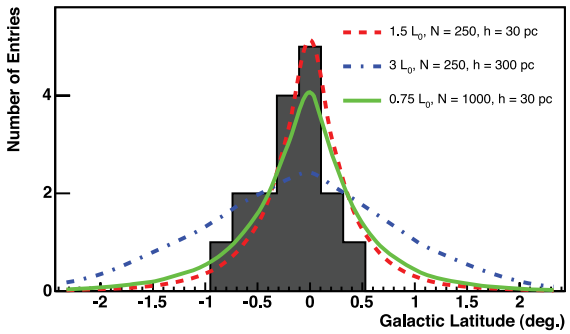


FIG. 23.—Comparison of the Galactic latitude distribution of the VHE gamma-ray sources in the survey region with the prediction of a simple source population model assuming scale heights in the Galactic disk of 30 (*red and green lines*) and 300 pc (*blue line*). The sources are assumed to be monoluminous. The lines are not normalized and give the predicted number of detected sources in each latitude bin taking into account the reduced sensitivity at higher latitudes (Fig. 3). The legend gives the physical parameters in each case with $L_0 = 1.3 \times 10^{34}$ ergs s$^{-1}$ (in the energy range 0.2–10 TeV) as previously defined. $N$ denotes the number of expected gamma-ray sources.

1 cm$^{-3}$ $< n <$ 10 cm$^{-3}$. Figure 23 shows the expected distributions from this simple model for a scale height in the Galactic disk of 30 (*red line*) and 300 pc (*blue line*). The green line is the same as the red line but with 4 times as many sources, each with half the luminosity, illustrating the relative insensitivity of the shape of the distribution on the assumed source luminosity distribution. The difference between the blue and the red line illustrates that the H.E.S.S. survey has a broad enough sensitive coverage in $b$ to distinguish these two scenarios. For the 300 pc line (*blue line*), an intrinsic luminosity twice that of the 30 pc case has been assumed to give reasonable agreement with the number of detected sources. As can be seen from Figure 23, the experimental data favor a scale height for the parent population of $<$100 pc in line with expectations for young SNRs and PWNs or massive star forming regions.

## 7. CONCLUSIONS

The inner part of our Galaxy now contains 17 known sources of VHE gamma rays, compared to three before the H.E.S.S. survey. The increased number of sources allows us to consider the behavior of *populations* of sources for the first time in this wave band. A major task of multiwavelength follow-up observations and archival searches now lies ahead to understand the processes at work in these astrophysical particle accelerators. The paradigm of cosmic-ray acceleration in SNRs is consistent with our new findings, but it seems clear that the new sources are not drawn from a single population. Follow-up observations of the new sources with H.E.S.S. are planned, as well as an extension of this survey into unexplored regions of the Galactic plane.

The support of the Namibian authorities and of the University of Namibia in facilitating the construction and operation of H.E.S.S. is gratefully acknowledged, as is the support by the German Ministry for Education and Research (BMBF), the Max Planck Society, the French Ministry for Research, the CNRS-IN2P3 and the Astroparticle Interdisciplinary Programme of the CNRS, the UK Particle Physics and Astronomy Research Council (PPARC), the IPNP of Charles University, the South African Department of Science and Technology and National Research Foundation, and the University of Namibia. We appreciate the excellent work of the technical support staff in Berlin, Durham, Hamburg, Heidelberg, Palaiseau, Paris, Saclay, and Namibia in the construction and operation of the equipment. We thank Y. Uchiyama for assistance with the *ASCA* analysis. This research has made use of data obtained from the High Energy Astrophysics Science Archive Research Center (HEASARC), provided by NASA's Goddard Space Flight Center.

## REFERENCES

Aharonian, F., Atoyan, A. M., & Kifune, T. 1997a, MNRAS, 291, 162
Aharonian, F., Hofmann, W., Konopelko, A. K., & Völk, H. J. 1997b, Astropart. Phys., 6, 343
———. 1997c, Astropart. Phys., 6, 369
Aharonian, F., et al. 2002a, A&A, 393, L37
———. 2002b, A&A, 395, 803
———. 2004a, A&A, 425, L13
———. 2004b, Astropart. Phys., 22, 109
———. 2004c, Nature, 432, 75
———. 2005a, A&A, 430, 865
———. 2005b, A&A, 432, L25
———. 2005c, A&A, 437, L7
———. 2005d, A&A, 439, 1013
———. 2005e, A&A, in press
———. 2005f, Science, 307, 1938
———. 2005g, Science, 309, 746
Amenomori, M., et al. 2002, ApJ, 580, 887
Atkins, R., et al. 2004, ApJ, 608, 680
Bamba, A., Ueno, M., Koyama, K., & Yamauchi, S. 2003, ApJ, 589, 253
Baring, M. G. 2004, Adv. Space Res., 33, 552
Benaglia, P., Romero, G. E., Stevens, I. R., & Torres, D. F. 2001, A&A, 366, 605
Berezhko, E. G., & Völk, H. J. 1997, Astropart. Phys., 7, 183
———. 2000, A&A, 357, 283
Bernlöhr, K., et al. 2003, Astropart. Phys., 20, 111
Bertsch, D. L., et al. 2000, in AIP Conf. Proc. 510, The 5th Compton Symposium, ed. M. L. McConnell & J. M. Ryan (New York: AIP), 504
Blandford, R., & Eichler, D. 1987, Phys. Rep., 154, 1
Blondin, J. M., Chevalier, R. A., & Frierson, D. M. 2001, ApJ, 563, 806
Brogan, C. L., Gaensler, B. M., Gelfand, J. D., Lazendic, J. S., Lazio, T. J., Kassim, N. E., & McClure-Griffiths, N. M. 2005, ApJ, 629, L105
Bronfman, L., Casassus, S., May, J., & Nyman, L.-A. 2000, A&A, 358, 521
Case, G., & Bhattacharya, D. 1996, A&AS, 120, 437C
Cheng, K. S. 2004, Adv. Space Res., 33, 561
Churchwell, E. 1990, A&A Rev., 2, 79
Combi, J. A., Benaglia, P., Romero, G. E., & Sugizaki, M. 2005, A&A, 431, L9
Cornils, R., et al. 2003, Astropart. Phys., 20, 129
Dame, T. M., Hartman, D., & Thaddeus, P. 2001, ApJ, 547, 792
Dame, T. M., & Thaddeus, P. 1994, ApJ, 436, L173
de Naurois, M., et al. 2002, ApJ, 566, 343
Dickey, J. M., & Lockman, F. J. 1990, ARA&A, 28, 215
Drury, L. O'C, Aharonian, F., & Völk, H. J. 1994, A&A, 287, 959
Enomoto, R., et al. 2002, Nature, 416, 823
Finley, J. P., & Ögelman, H. 1994, ApJ, 434, L25
Fleysher, R., et al. 2005, in AIP Conf. Proc. 745, International Symposium on High-Energy Gamma-Ray Astronomy, ed. F. A. Aharonian, H. J. Völk, & D. Horns (New York: AIP), 269
Funk, S., et al. 2004, Astropart. Phys., 22, 285
Gaensler, B. M., & Johnston, S. 1995, MNRAS, 275, L73
Gaensler, B. M., Schulz, N. S., Kaspi, V. M., Pivovaroff, M. J., & Becker, W. E. 2003, ApJ, 588, 441
Ginzburg, V. L., & Syrovatskii, S. I. 1964, The Origin of Cosmic Rays (New York: Macmillan)
Green, A. J., Cram, L. E., Large, M. I., & Ye, T. 1999, ApJS, 122, 207
Green, D. A. 2004, Bull. Astron. Soc. India, 32, 335
Hall, T. A., et al. 2003, in Proc. 28th Int. Cosmic Ray Conf. (Tsukuba), 2497
Hartman, R. C., et al. 1999, ApJS, 123, 79
Haschick, A. D., & Ho, P. T. P. 1983, ApJ, 267, 638
Helfand, D. J., Becker, R. H., & White, R. L. 2005, ApJ, submitted (astro-ph/0505392)
Hinton, J. A. 2004, NewA Rev., 48, 331
Hirotani, K. 2001, ApJ, 549, 495
Jones, F. C., Lukasiak, A., Ptuskin, V., & Webber, W. 2001, ApJ, 547, 264
Kassim, N. E. 1992, AJ, 103, 943
Kassim, N. E., & Weiler, K. W. 1990, Nature, 343, 146

Kassim, N. E., Weiler, K. W., & Baum, S. A. 1991, ApJ, 374, 212
Kastner, J. H., Balick, B., Blackman, E. G., Frank, A., Soker, N., Vrtílek, S. D., & Li, J. 2003, ApJ, 591, L37
Koyama, K., Petre, R., Gotthelf, E. V., Hwang, U., Matsuura, M., Ozaki, M., & Holt, S. S. 1995, Nature, 378, 255
Li, T.-P., & Ma, Y.-Q. 1983, ApJ, 272, 317
Malizia, A., et al. 2004, in Proc. 5th *INTEGRAL* Workshop on the *INTEGRAL* Universe, ed. V. Schönfelder, G. Lichti, & C. Winkler (ESA SP-552; Noordwijk: ESA), 161
Malkov, M. A., & Drury, L. O'C. 2001, Rep. Prog. Phys., 64, 429
Manchester, R. N., Hobbs, G. B., Teoh, A., & Hobbs, M. 2005, AJ, 129, 1993
Montmerle, T. 1979, ApJ, 231, 95
Nolan, P. L., Tompkins, W. F., Grenier, I. A., & Michelson, P. F. 2003, ApJ, 597, 615
Ojeda-May, P., Kurtz, S. E., Rodríguez, L. F., Arthur, S. J., & Velázquez, P. 2002, Rev. Mex. AA, 38, 111
Paladini, R., Burigana, C., Davies, R. D., Maino, D., Bersanelli, M., Cappellini, B., Platania, P., & Smoot, G. 2003, A&A, 397, 213
Parizot, E., Marcowith, A., van der Swaluw, E., Bykov, A. M., & Tatischeff, V. 2004, A&A, 424, 747
Patel, S. K., et al. 2004, ApJ, 602, L45
Reimer, O., & Bertsch, D. L. 2001, in Proc. 27th Int. Cosmic Ray Conf. (Hamburg), 2546
Revnivtsev, M., Tuerler, M., Del Santo, M., Westergaard, N. J., Gehrels, N., & Winkler, C. 2003, IAU Circ., 8097, 2
Reynoso, E. M., & Mangum, J. G. 2000, ApJ, 545, 874
Rodriguez, J., Tomsick, J. A., Foschini, L., Walter, R., Goldwurm, A., Corbel, S., & Kaaret, P. 2003, A&A, 407, L41
Rowell, G. P. 2003, A&A, 410, 389
Smith, A. J., et al. 2005, in AIP Conf. Proc. 745, International Symposium on High-Energy Gamma-Ray Astronomy, ed F. A. Aharonian, H. J. Völk, & D. Horns (New York: AIP), 657
Sugizaki, M., Mitsuda, K., Kaneda, H., Matsuzaki, K., Yamauchi, S., & Koyama, K. 2001, ApJS, 134, 77
Thompson, D. J., Bertsch, D. L., & O'Neal, R. H., Jr. 2005, ApJS, 157, 324
Tomsick, J. A., Lingenfelter, R., Walter, R., Rodriguez, J., Goldwurm, A., Corbel, S., & Kaaret, P. 2003, IAU Circ., 8076, 1
Torii, K., et al. 1998, ApJ, 494, L207
Ubertini, P., et al. 2005, ApJ, 629, L109
Vincent, P., et al. 2003, in Proc. 28th Int. Cosmic Ray Conf. (Tsukuba), 2887
Vink, J. 2004, ApJ, 604, 693
Völk, H. J., Berezhko, E. G., & Ksenofontov, L. T. 2003, A&A, 409, 563
Völk, H. J., & Forman, M. 1982, ApJ, 253, 188
Weekes, T. C. 2000, in AIP Conf. Proc. 558, International Symposium on High-Energy Gamma-Ray Astronomy, ed. F. A. Aharonian & H. J. Völk (New York: AIP), 15
Weekes, T. C., et al. 1989, ApJ, 342, 379
Weisskopf, M. C., et al. 2000, ApJ, 536, L81
White, R. L. 1985, ApJ, 289, 698
White, R. L., Becker, R. H., & Helfand, D. J. 2005, AJ, 130, 586
Whiteoak, J. B. Z., & Green, A. J. 1996, A&AS, 118, 329